EXAMENSARBETE INOM MASKINTEKNIK,
AVANCERAD NIVÅ, 30 HP

STOCKHOLM, SVERIGE 2020

Analysis and Initial Optimization of The Propeller Design for Small, Hybrid-Electric Propeller Aircraft

Analys och Initial Optimering av Propellern Design för Små, Hybrid- Eldrivet Propeller Flygplan

ALI ALSHAHRANI

KTH
SKOLAN FÖR TEKNIKVETENSKAP

Authors

Ali Alshahrani <alialsh@kth.se>
Aeronautical and Vehicle Engineering
KTH Royal Institute of Technology

Place for Project

Stockholm, Sweden
Main Campus

Examiner

Dr Raffaello Mariani
KTH Royal Institute of Technology

Supervisor

The Supervisor
Dr Raffaello Mariani
KTH Royal Institute of Technology

Abstract

This thesis focuses on the optimization of the electric aircraft propeller in order to increase flight performance. Electric aircraft have limited energy, particularly the electric motor torque compared to the fuel engine torque. For that, redesign of the propeller for electric aircraft is important in order to improve the propeller efficiency. The airplane propeller theory for Glauert is selected as a design method and incorporated with Bratt improvements of the theory. Glauert theory is a combination of the axial momentum and blade element theory. Pipistrel Alpha Electro airplane specifications have been chosen as a model for the design method. Utilization of variable pitch propeller and the influence of number of blades has been investigated. The obtained design results show that the variable pitch propellers at cruise speed and altitude 3000 m reducing the power consumption by 0.14 kWh and increase the propeller efficiency by 0.4% compared to the fixed pitch propeller. Variable pitch propeller improvement was pretty good for electric aircraft. The optimum blade number for the design specifications is 3 blades.

Keywords

Electric, hybrid, Propeller, Optimization, variable pitch, fixed pitch, blades number.

Sammanfattning

Denna rapport har som fokus att optimera propellern på ett eldrivet flygplan för att förbättra flygprestationen. Eldrivna flygplan har begränsad energi, i synnerhet motorns vridmoment i jämförelse med bränslemotorns vridmoment. Därav behöver propellern designas om för att uppnå en större verkningsgrad i propellern. Glauerts teori om flygplanspropellrar har använts som metod för designen där vissa modifieringar i teorin har tillämpats enligt Bratt för att förbättra teorin. Glauerts teori är en kombination mellan axiell momentum- och bladelement teori. Specifikationerna för Pipistrel Alpha Electro flygplan har använts som modell i design metoden. Utnyttjande av propeller med justerbara bladvinklar samt antal blads påverkan har undersökts. De erhållna designresultaten visade att propellern med justerbara bladvinklar vid planflykt på 3000 m höjd har sparat 0,14 kWh samt ökat propellerns verkningsgrad med 0,4% jämfört med propellern med icke justerbara bladvinklar. Propeller med justerbara stigning var lämplig för elflygplan. Det optimala antalet blad för designspecifikationerna är 3 blad.

Nyckelord

Eldrivet, hybrid, Propeller, Optimering, justerbar vinkel, fast vinkel, bladnummer.

Acknowledgement

I would like to thank Dr. Raffaello Mariani, my supervisor, for his help, and he has always been the guide and the leader for my work.

I wish to express my sincere gratitude to my parents for their support and continuous encouragement.

Special thanks go to Huawei Technologies consultant Prof. Jamil Ahmed, who has helped me to improve the design code.

I also want to thank KTH library, who has supported me with the references that I needed in the research.

Nomenclature

η_c	Cruise efficiency of the propeller, N
η_P	Propeller efficiency
ρ	Air density, kg/m^3
σ	Propeller Solidity
a	Sound speed, m/s
AR	Aspect ratio of the wing
C	Blade chord, m
C_{D_i}	Induce drag coefficient
C_L	Lift coefficient
C_Q	Torque coefficient
C_{D_0}	Zero lift Drag coefficient
$C_{L_{max}}$	Maximum lift coefficient
D	Propeller Diameter, m
e	Efficiency factor where $e < 1$
E_{TOT}	Total energy of the battery, kW
g	Earth gravity, m/s^2
H	Blade thickness, m
K_T	Reduction factor from drag fraction and tip losses

K_X Leans factor

M Mach number

P Engine Power, w

q Dynamic pressure, pa

R Propeller radius, m

RPM Revolution Per Minute

RPS Revolution Per Second

S Wing span, m

T Propeller thrust, N

T_c Cruise thrust of the propeller, N

V_0 Forward airspeed of the aircraft, m/s

V_c Cruise speed of the aircraft, m/s

V_y Aircraft speed of maximum ROC, m/s

W Aircraft weight, Kg

Z Number of blades

Subscripts

AC Aircraft

av Available

c Cruise

req Required

Contents

Chapter 1

Introduction

1.1 Background

Since the invention of airplanes,combustion engines were utilized. Over the decades, the combustion engines developed and became more efficient, and produced a high level of energy per kilogram of fuel. Nonetheless, the emission footprint of these engines still threatens the environment where fuel consumption in aviation contributes around 2% to 3% of global CO_2 emissions [1]. Using an electric propulsor instead of a combustion engine in order to reduce CO2 emission becomes more necessary, particularly with the industry evolution of electric motors.

In the meantime, the electric motors have light weight and high speed of rotation compared to the combustion engines that minimizes the need for gearboxes [2]. Also, it does not need air to produce power that makes the engine reach full energy even at high altitudes.

The advantages of electric aircraft are varied. On the finance side, the lower cost of electrical energy compared to fossil fuel. And for the pollution, noise and exhaust emissions are reduced compared with combustion engines. Besides, Electric motors have much higher efficiency relative to combustion engines [3]. Maximum electric motor torque is instantaneous, while in piston engine needs several thousand RPM to reach the maximum torque [4]. Additionally, take advantage of the propeller rotation to generate power and recharge the battery. The center of gravity of electric aircraft is stationary due to the fixed weight during flight.

Nevertheless, electric propulsion still faces many difficulties, such as fixed battery weight during the flight, and large mass and volume storage. Currently, 1 kg of jet fuel contains around 25 to 30 times energy more than battery [2]. Therefore, electric propulsion

applications are limited to small aircraft and short-distance travel [5]. Otherwise, hybrid-electric aircraft is an option for commercial aircraft that combines gas turbine engines with electric propulsion systems. High required power at take-off and climb is another reason to use hybrid-electric aircraft.

1.2 Problem statement

The energy of batteries is limited, and it is beneficial to develop electric aircraft with high efficiency. The propulsion efficiency is affected by the motor, the controller, and the propeller. It is mainly affected by the propeller efficiency, and that attribute to the propeller has a narrow high efficiency operating range, while the motor and the controller are capable of high efficiency operation through the entire flight [6, 7]. Most of the existing propellers were designed for the combustion fuel engines that are usually used to operate the electric aircraft without adjustments on the design, while the electric motor torque is limited compared to the fuel engine torque. This is an essential reason to redesign the propeller for the electric aircraft in order to improve propeller efficiency, which enhances the endurance of the aircraft [8, 9].

1.3 Purpose

The objective of this study is to perform a design optimization for an electric aircraft propeller in order to improve the performance. This objective can be achieved by the following steps:

1- Design a fixed pitch propeller for the Pipistrel Alpha Electro powered by 60-kW electric motor via airplane propeller theory for Glauert [10].

2- Investigate the performance of the RAF 6 airfoil used for aircraft propellers.

3- Calculate the airplane performance at max take-off weight of 550 Kg for the proposed flight condition.

4- Observe the improvement of variable pitch parameter on the performance at the same flight condition.

5- Observe the blade number influence on performance, which has not been investigated before for an electric aircraft propeller.

Chapter 2

Background theory and related Work

2.1 Electric and hybrid-electric aircraft

Over the past two decades, research focused on improving and developing electric and hybrid-electric aircraft by utilizing various methods in order to maximize and optimize the range of flight. Ma et al. [6] improved the efficiency of an electric aircraft propulsion system by solving an optimization problem by minimizing the energy consumption per flight. They investigated the method via experiment on a two-seater electric aircraft and demonstrated reducing the energy consumption of the electric aircraft by over 10%. Solar Impulse manufactured a solar-powered electric aircraft, where the solar cells charge the battery to maintain sustainable flight [11]. Glassock et al. [12] applied a study on hybrid-electric aircraft used for skydiving missions in order to reduce fuel consumption. Takahashi et al. [13] displayed a new thrust control method for an electric aircraft propeller in order to improve safety.

Batteries are a critical parameter for long power supply to the electric motors. Lithium-ion batteries are widespread in electric aircraft propulsion applications because they have a high energy density and environmentally energy source. Yetik and Karakoc [14] performed a numerical thermal analysis for lithium-ion prismatic batteries to ensure the safety of hybrid-electric aircraft. Currently, the battery's energy capacity improved up to 400 Wh/kg [15].

2.2 Aircraft propeller design

Many scholars focused on improving and optimizing the design of the propeller. In 1919, A. Betz [16] demonstrated an approach to minimize the induced loss of a propeller. Based on Betz's work, Larrabee [17] showed a practical design for the propeller to calculate the

minimum induced loss. Goldstein [18] developed the vortex-theory of screw propellers and minimized the energy loss by solving the distribution of circulation along a propeller blade. Eppler and Hepperle [19] published the inverse method for propeller design that computes the propeller profiles from the given velocity distributions. Theodorsen [20] extended the tables of Goldstein circulation function and developed the theory of propellers with ideal load distribution. Wald [21] applied a practical design of propellers of minimum induced loss based on Theodorsen's work. D'Angelo et al. [22] presented an optimal numerical design for the propeller and validated experimentally by integrated two algorithms obtained from Vortex theory and Wing theory. Zheng et al. [23] proposed an approach based on Vortex Lattice Method (VLM) and Lifting Line Theory that can identify the optimal efficiency according to the design parameters, the number of propeller blades, blade radius, and rotation speed. Also, Cho and Lee [24] used VLM integrated with a Lifting Body Surface Theory (LBS) as a technique to optimize propeller blade shape for efficiency improvement. Lieser et al. [25] applied LBS and found out that noise reduction of the propeller could be achieved by diameter reduction, tip Mach number reduction, and by increasing the number of blades. The tip propeller blade shape also has little effects on the noise. Moreover, increasing the advance ratio gains more thrust for 6 blades propeller compare to 2 blades. Otherwise, at a low advance ratio, 2 blades propeller has more thrust.

2.3 Electric aircraft propeller design

Recently, some optimization research for electric aircraft propeller design has been investigated. Gur and Rosen [26] presented a new method to design an optimal propeller for an ultralight aircraft based on a multidisciplinary design optimization approach. This method contains the analysis for aerodynamics, acoustics, and structural analysis. Xiang et al. [27] proposed a design method combined with the genetic algorithm that obtains the optimal chord and pitch-angle of the propeller for a Li-ion battery-powered aircraft. Also, Xiang et al. [9] improved a design method for the propeller of electric aircraft according to the flight velocity, thrust, and rotation speed for cruise condition. A wind tunnel test was carried out for the propeller model and showed a good agreement with the numerical result. Stuhlpfarre et al. [28] performed numerical and experimental investigations of the propeller characteristics of ultralight aircraft. Two different numerical approaches have been used. First, simulation solving the unsteady Reynolds-averaged Navier–Stokes equations. Second, a blade element theory approach coupled with the Reynolds-averaged Navier–Stokes. Wu et al. [29] conducted a numerical and experimental study to investigate the noise reduction of an electric propeller aircraft. The study shows that aerodynamic noise can effectively be reduced by changing the blade shape along the spanwise at the same rotation speed, higher than 1000 rpm.

Chapter 3

Methods

3.1 Propeller design methodology

The airplane propeller theory from Glauert was selected as a design approach for the propeller due to the combination of the axial momentum and blade element theory in this method. The axial momentum theory considers the propeller as an actuator disk where the flow momentum changes by increasing the slipstream velocity in the axial direction from up-stream to down-stream of the propeller, as shown in Figure 3.1. It's developed by Rankine [30] in 1865 and improved in 1869 by Froude [31] who took the effects of slipstream rotation into account. This theory can be applied to predict the thrust and power performance. The blade element method introduces the performance profile distribution by elements along the blade and gives more details about the characteristics of the propeller. Also, Glauert simplified Goldstein's coefficient and included it in the performance calculation.
Furthermore, Bratt [32] improved the analysis for Glauert's theory, which is implemented in the design method for this work.

3.2 Initial propeller design

It is possible to predict the preliminary performance of the propeller with the help of non-dimensional coefficients. The performance of a propeller depends strongly on the relation between the airplane velocity V_0 and the angular velocity Ω of the propeller. Thrust is a function of forward speed V_0, RPM, and diameter. This function is expressed as the advance ratio (J), which measures the ratio of free-stream fluid speed (aircraft speed) to the propeller tip speed. The advance ratio is defined as follows:

$$J = \frac{V_0}{nD} = \frac{60 \cdot V_0}{RPM \cdot D} \tag{3.1}$$

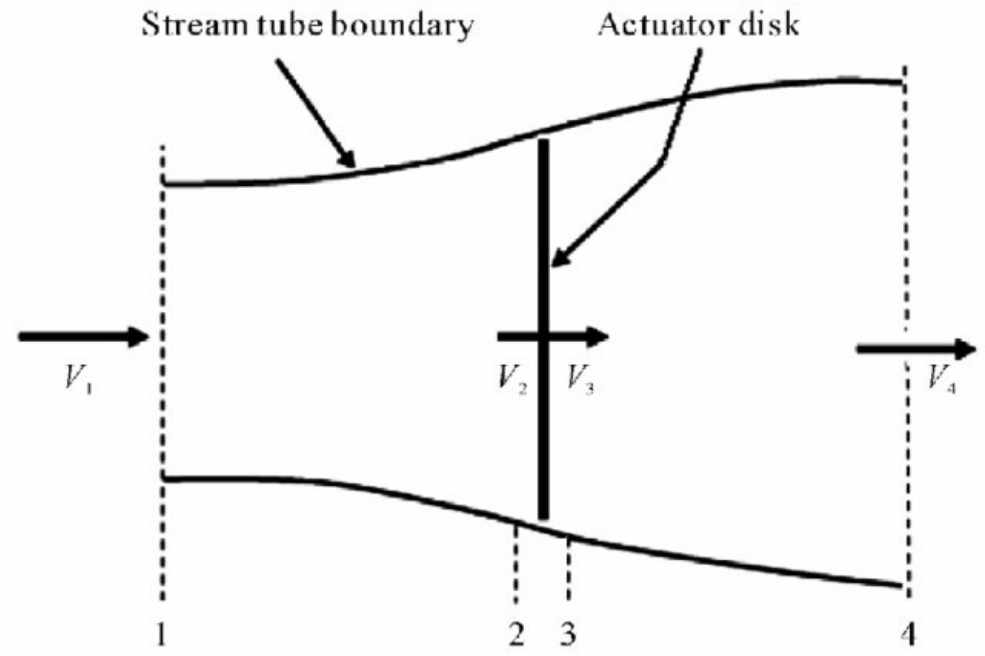

Figure 3.1: Actuator Disk.

Power and thrust coefficients combined with advance ratio to calculate the propeller efficiency are:

$$C_P = \frac{P}{\rho n^3 D^5} \tag{3.2}$$

$$C_T = \frac{T}{\rho n^2 D^4} \tag{3.3}$$

$$C_Q = \frac{Q}{\rho n^2 D^5} \tag{3.4}$$

Also, the thrust coefficient that can be detected from the propeller has been tested in a wind tunnel. For example, NACA published reports 640 and 650 [33, 34] of the propeller wind tunnel test that present diagrams for various airfoils for power and thrust coefficients with respect to the advance ratio as shown in Figure3.2.

Thus, propeller efficiency is:

$$\eta = \frac{TV_0}{P} = J\frac{C_T}{C_P} \tag{3.5}$$

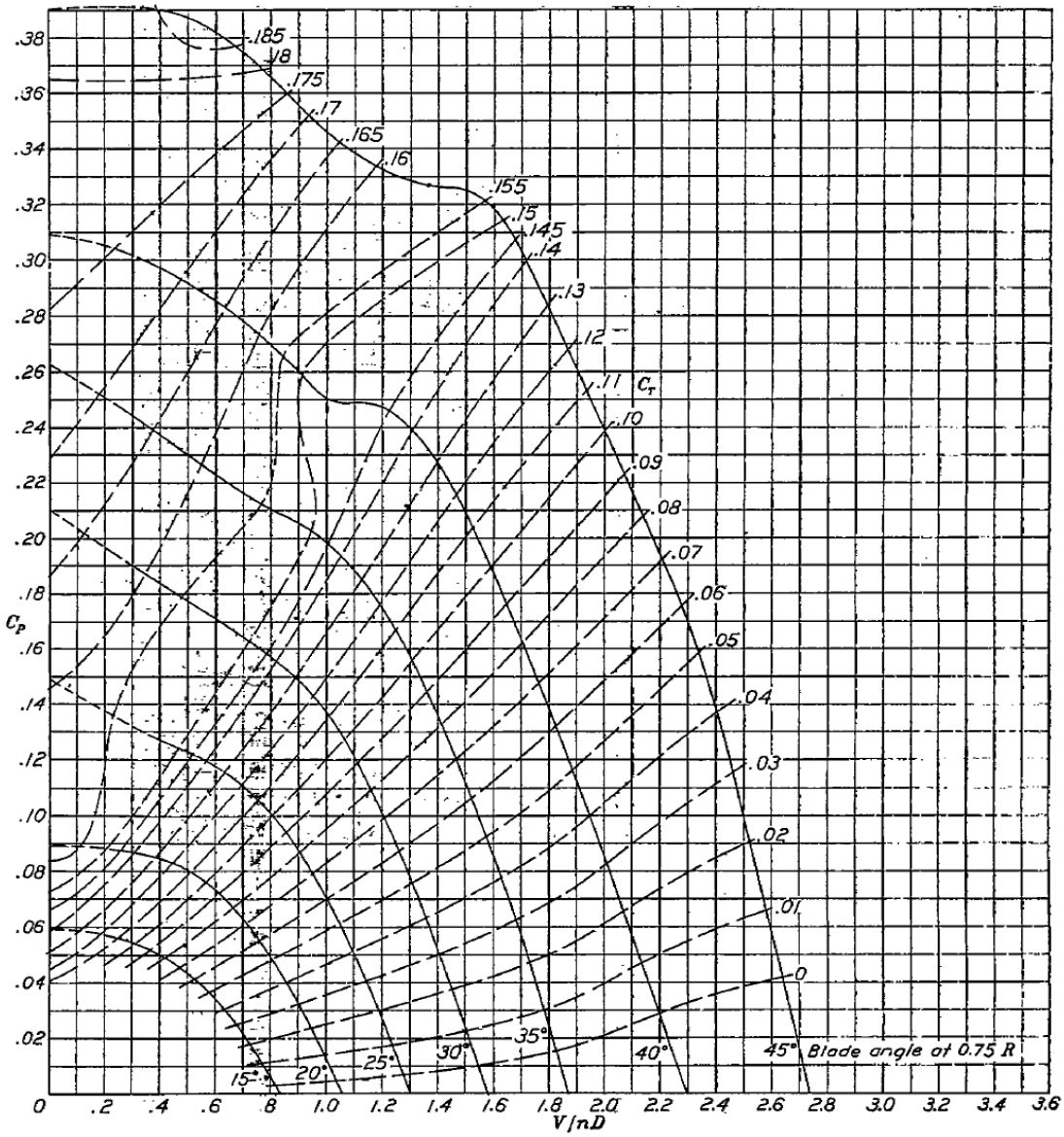

Figure 3.2: Power coefficient curves for propeller 5868-9 (Clark Y section) [34].

3.3 Design point

The propeller operates at various conditions, but to design a new propeller, there are two main cases which are required to be considered. These cases are: design point and arbitrary speed point [32]. The design point is the maximum performance of the propeller with full speed at sea level condition, and aircraft drag should be exactly the same as the thrust of the propeller at a maximum horizontal constant speed and full engine power. Cruise speed is considered as the arbitrary speed point in the design.

3.4 Propeller angels and speeds definitions

Blade element theory based on dividing the propeller blade into elements with width *dr* and calculate the characteristics of each element. The angles and speeds are defined at blade element *dr* on the distance from center *r*, as shown in Figure 3.3. Figure 3.4 shows cross section of the blade element *dr*. The angles and speeds are identified in Table 3.1.

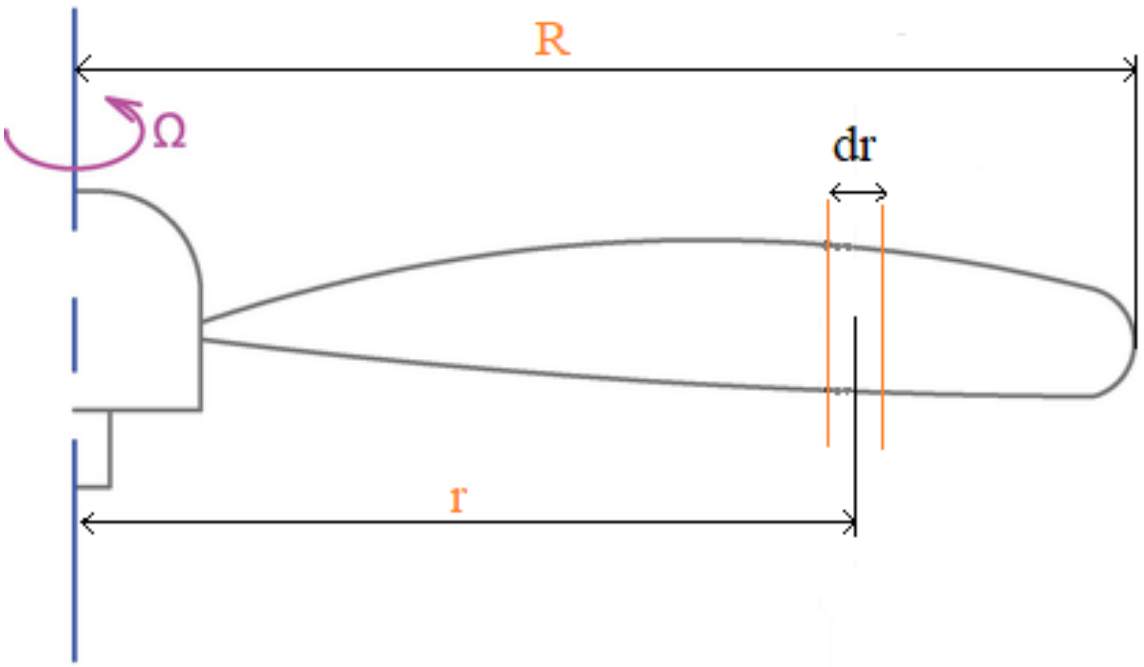

Figure 3.3: Definition of propeller geometry [35].

3.5 Goldstein coefficient

Goldstein's coefficient *K* is related to the top losses of the propeller for a finite number of blades. The principle is that induced speed *W* of the ring element is less than the mean value of the induced speed W_m, and the coefficient calculates this variance K=W_m/W. Goldstein's coefficient *K* is a unique function of sin (ϕ_i) and relative station ($X = r/R$). The method to calculate *K* is:

1- Calculate the angular speed of the slipstream (O_2), where the propeller forces the slipstream to move backwards and rotate.

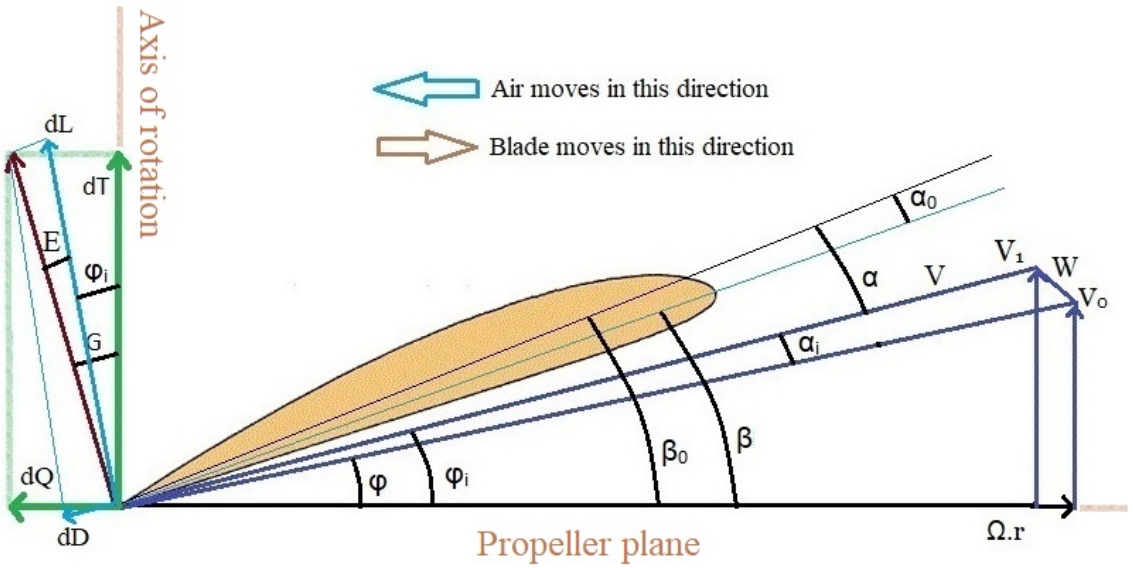

Figure 3.4: Definition of the velocity, angles, and forces at Cross section of the blade.

$$O_2 = \frac{(r * \Omega - ((r * \Omega)^2 - 4 * V_1 * (V_1 - V_0))^{\frac{1}{2}})}{r} \tag{3.6}$$

2- Calculate ϕ_i and *K* function factor *S* at *X* and at the blade tip, called S_2.

$$\phi_i = tan^{-1}[\frac{0.5 * r * O_2}{(V_1 - V_0)}] \tag{3.7}$$

$$S = sin(\phi_i) \tag{3.8}$$

$$S_2 = \frac{X * S}{(1 - (1 - X^2) * S^2)^{\frac{1}{2}}} \tag{3.9}$$

3- Calculate the exponent to approximate *K*.

$$F = \frac{\frac{Z}{2*(1-X)}}{S_2} \tag{3.10}$$

4- Calculate an approximate value of *K* called K_1.

$$K_1 = \frac{Z}{\pi * cos^{-1}(e^{-F}) * \frac{\pi}{180}} \tag{3.11}$$

5- Calculate the exponent for approximate *K* at *K* function factor *S*=1.

$$F_2 = \frac{Z}{2 * (1 - X)} \tag{3.12}$$

Table 3.1: Parameters definitions at cross-sectional view of blade element.

Symbol	**Definition**
dT	Thrust
dQ	Torque / radius
dL	Lift
dD	Drag
r	Arbitrary distance from center to blade element
Ω	Angular velocity of the propeller
Ω.r	Element blade speed
V_0	Forward airspeed of the aircraft
V_1	Slipstream speed
V	Inflow speed
W	Induced speed
ϕ	Angle of advance
ϕ_i	Inflow angle
β	Blade pitch angle
β_0	Zero lift blade angle
α	Angle of attack
α_0	Zero lift angle of the airfoil
α_i	Induced angle of attack
G	Load/thrust ratio angle
E	Drag/lift ratio angle

6- Calculate approximate *K* for *S*=1 called K_2.

$$K_2 = \frac{cos^{-1}(e^{-F_2})}{90} \tag{3.13}$$

7- The number of blades affects the value of *K*. Therefore, the equations differ based on the number of blades. For 2 blades:

K for *S*=1:

$$N = \frac{(1 - X^2)^{1/2}}{\pi * X} \tag{3.14}$$

K for *S* at relative station *X*:

$$K = K_1 - (K_2 - N) * S^{(X-S)} \tag{3.15}$$

For 3 blades:
K for *S*=1:

$$N_2 = \frac{4}{\pi^2 * log(\frac{1}{X^2} + (\frac{1}{X^4-1})^{1/2})} \tag{3.16}$$

K for *S* at relative station *X*:

$$K = K_1 - (K_2 - N_2) * S^{(X-S)} \tag{3.17}$$

For 4 blades:
Kappa for *S*=1:

$$N_3 = \frac{N + N_2}{2} \tag{3.18}$$

Kappa for *S* at relative station *X*:

$$K = K_1 - (K_2 - N_3) * S^{(X-S)} \tag{3.19}$$

3.6 Airfoil selection

Two types of airfoil sections are essential for the propeller, which are the straight lower surface section, and the convex lower surface section [32]. Clark Y and RAF 6 airfoils are commonly used as a propeller aerofoil [34, 36]. RAF 6 airfoil started early design but has given way for Clark Y airfoil recently, and that attributes to the low minimum drag and the low maximum lift of Clark Y airfoil. Clark Y airfoil is a straight lower surface but bent from the leading edge to 0.2 of the chord, and RAF 6 airfoil is a straight lower surface from the leading edge to the trailing edge, as shown in Figure 3.5.

Figure 3.5: Clark Y and RAF 6 airfoils sections for 10% thickness [33].

Zero lift angle formula for Clark Y airfoil differs from RAF 6 airfoil formula. Where Clark Y formula:

$$\alpha_0 = 40 * (\frac{H}{C}) + 1 \tag{3.20}$$

and RAF 6 formula:

$$\alpha_0 = 43 * (\frac{H}{C}) \tag{3.21}$$

3.7 Aerodynamics blade loads

The air loads on the propeller for element blade theory divided to thrust load *T*, which gives the forward speed for the airplane, and torque loads *Q* and that balanced by the engine torque. From Figure 3.1, the mass flow passing through a blade element ring *dr* and with consideration of Goldstein's coefficient *K* the thrust for one blade element will be:

$$dT_1 = 2 * \pi * r * dr * \rho * V_1 * (V_1 - V_0) * K \tag{3.22}$$

Also, from Figure 3.4 the thrust for a blade element ring *dr* will be:

$$dT_2 = \frac{dQ}{tan(G)} \tag{3.23}$$

Where *dQ* is the torque of the ring elements of one blade propeller, and its value is an estimated value with condition $dT_1 = dT_2$ and balance with V_1, value where $V_1 > V_0$. The term V_1 is an estimated value that gives a value of *dQ* load corresponding to the *dQ* from the engine torque. Also, It is not recommended to have a high value of *dQ* load distribution at blade tip because that may cause a stall at the inner part of the blade at zero and low speeds.

Based on the balance torque, engine torque that drives the propeller should always have the same propeller torque loads. In other words, the integrated value of *dQ* along one blade propeller should be the same as the engine torque value Q_0:

$$\int_0^R dQ * dr = \Sigma(dQ * dr * R) = Q_0 \tag{3.24}$$

$$Q_0 = \frac{P * 10^2 * g}{(Z * \Omega * CG)} \tag{3.25}$$

Center of gravity position of *dQ* area along the blade propeller is calculated by the following equation:

$$CG = \frac{\Sigma(dQ * r)}{\Sigma(dQ)} \tag{3.26}$$

Figure 3.4 shows *G*=ϕ_i+*E* where ϕ_i equation mentioned in Goldstein's coefficient section and *E* is the aerodynamic glide slope angle, so:

$$E = tan^{-1}(\frac{C_{D_0}}{C_L}) \tag{3.27}$$

$$C_L = \frac{4 * K * tan^{-1}(\alpha_i) * S}{\sigma} \tag{3.28}$$

$$\sigma = \frac{C * Z}{(2 * \pi * r)} \tag{3.29}$$

Drag coefficient computed as a function of C_L and relative thickness H/C.

$$C_{D_0} = \frac{6.25 * \frac{H}{C} + \frac{0.42625}{1.55 - C_L}}{100} \tag{3.30}$$

Maximum lift coefficient computed as a function of mach number.

$$C_{L_{max}} = -2.38333 * M^2 + 0.955 * M + 1.4 \tag{3.31}$$

$$M = \frac{V}{a} \tag{3.32}$$

$$V = \frac{V_1}{sin(\phi_i)} \tag{3.33}$$

3.8 Blade angle

From Figure 3.4, the blade angle is defined as:

$$\beta = \beta_0 - \alpha_0 \tag{3.34}$$

and

$$\beta_0 = \phi_i + \alpha \tag{3.35}$$

The propeller is producing the thrust with the same principle of the aircraft wing lift. Therefore, the angle of attack can be a function of the lift coefficient [32]:

$$\alpha = 9 * C_L \tag{3.36}$$

Total thrust of the propeller can be calculated by integrating the dT loads along the blade as follow:

$$\int_0^R dT * dr = \Sigma(dT * dr * R) \tag{3.37}$$

where:

$$dT = dT_1 = dT_2 \tag{3.38}$$

Thrust for the whole propeller:

$$T = Z * \Sigma(dT * dr * R) * 10 \tag{3.39}$$

And total propeller efficiency:

$$\eta_P = \frac{T * V_0}{P} \tag{3.40}$$

3.9 Interference between propeller and body

Aircraft body drag increases due to the propeller slipstream speed, which leads to decrease in thrust, and that means a reduction in the velocity which requires reducing the blade angle.

Propeller drag reduction can be calculated based on zero lift aircraft drag area f_0. It may be estimated that f_0= 0.4 m^2 which is common for light aircraft of normal good aerodynamic shape [32]. Also, the front part of the aircraft body only feels slipstream speed V_1 and causing drag. Therefore, V_1 needs to be recalculated as follow:

$$V_1 = \frac{V_0}{2} + \sqrt{(\frac{V_0}{2})^2 + \frac{T}{(0.5 * \pi * D^2 * \rho * K)}} \tag{3.41}$$

The slipstream speed behind the propeller will be

$$V_2 = 2 * V_1 - V_0 \tag{3.42}$$

The increased velocity from V_1 to V_2

$$V_{incr} = \frac{(V_1 + V_2)}{2} \tag{3.43}$$

The increased pressure

$$q_{incr} = \rho * \frac{V_{incr}^2}{2} \tag{3.44}$$

Aircraft drag in free stream air

$$D_{AC,incr} = f_0 * q_{incr} \tag{3.45}$$

Zero-lift drag of the aircraft

$$q = \rho * \frac{V_0^2}{2} \tag{3.46}$$

$$D_{0,AC} = f_0 * q \tag{3.47}$$

It may be assumed that 40% of the total aircraft drag will affect the increase of slipstream velocity. Thus, total drag for the propeller and aircraft is:

$$D_{tot} = 0.6 * D_{0,AC} + 0.4 * D_{AC,incr} \tag{3.48}$$

Increased drag by the aircraft body

$$D_{incr} = D_{tot} - D_{0,AC} \tag{3.49}$$

And the corrected thrust

$$T_{corr} = T - D_{incr} \tag{3.50}$$

3.10 Corrected blade angle

From Figure 3.4, reduce velocity means the angle of attack α will increase. Therefore, assume the change of blade angle β approximately as the change of *G* [32].

By apply the resultant torque Q_0 for the whole propeller, *G* for free propeller (without a body) will be:

$$G_0 = tan^{-1}(\frac{Q_0}{T}) \tag{3.51}$$

G for propeller in front of the body

$$G_2 = tan^{-1}(\frac{Q_0}{T_{corr}}) \tag{3.52}$$

Thus, reducing angle of β

$$\Delta\beta = G_0 - G_2 \tag{3.53}$$

Where the reduction of $\Delta\beta$ applies on all β angles of the elements along the blade.

3.11 Propeller at low and zero forward air speed

Fixed pitch propeller has a fixed blade angle. Therefore, compute the blade angle at the design point and change the other parameters such as engine power, RPM, and angle of

attack for any arbitrary aircraft speed "off design point". For off design, the true angle of attack occurs at $C_{L_1} = C_{L_2}$ and implementing that by adjusting V_1 [32].

$$C_{L_1} = \frac{4 * K * tan^{-1}(\alpha_i) * S}{\sigma} \tag{3.54}$$

$$C_{L_2} = \frac{\alpha}{9} \tag{3.55}$$

The case at zero forward airspeed is called a static case, and it is important for the aircraft take-off performance. Glauert method is less accurate in thrust calculation at static case due to the high lift coefficient, and partly or totally stall over the propeller blade. However, this issue can solve by the following methods set:

1- Bendemann formula is an approximated method that calculates a reliable static thrust (assuming aircraft speed equal zero). But Bendemann did not pay attention to blade friction and other losses which are considered in the calculation [32].

$$T_{static} = K_T * (0.5 * P^2 * \rho * \pi * D^2)^{0.333} \tag{3.56}$$

2- Using a thrust coefficient that is measured based upon wind tunnel tests to calculate static thrust. For example, Figure 3.6 is based upon wind tunnel tests, at low and zero speed C_T in the region of 0.1 to 0.12 [33]. Thrust is then:

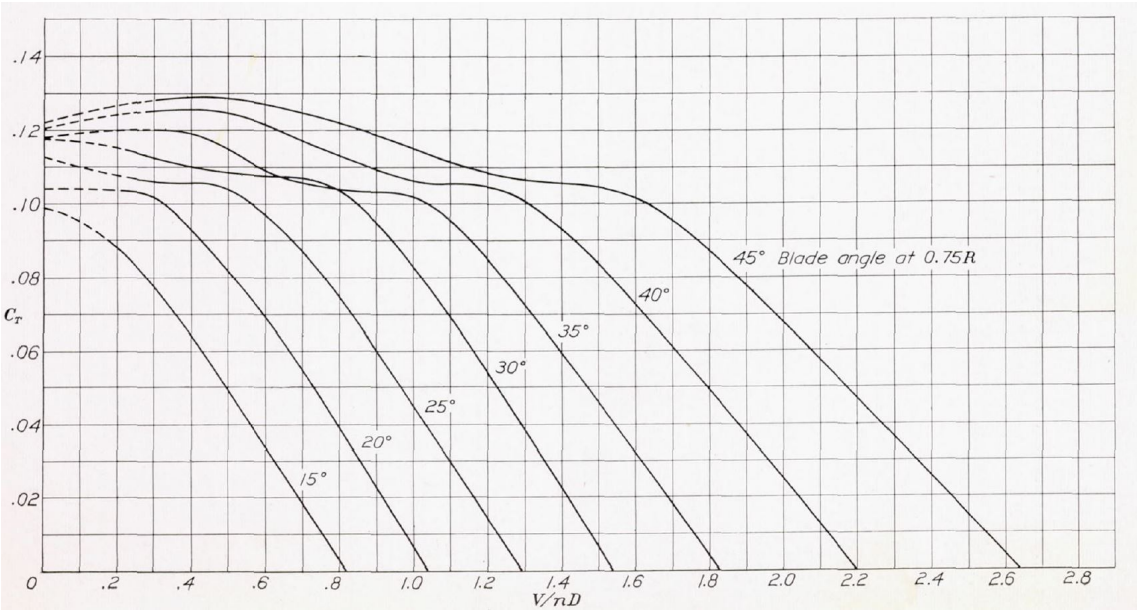

Figure 3.6: Thrust coefficient curves for propeller 5868-9 (Clark Y section), 2 blades [33].

$$T_{static} = C_T * \rho * RPS^2 * D^4 \tag{3.57}$$

3- Bratt method to calculate static thrust based on the resultant of *dQ* and *dT*. This method is the most accurate compared to Bendemann formula and thrust coefficient measurement. This method uses the same approach used in section 3.7 but with modifying the calculation way of drag/lift ratio angle *E*.

$$E = K_X * \alpha \tag{3.58}$$

$$K_X = 0.275 * (1 + \frac{H}{C})^4 \tag{3.59}$$

The efficiency for the propeller is zero when the aircraft speed V_0 equals zero. For that, Utilizing the mean value of V_1 instead of V_0 to calculate a static Figure of merit.

$$Fm = \frac{T * V_1}{P} \tag{3.60}$$

3.12 Performance analysis of the aircraft

The purpose of the analysis is to estimate the available thrust for a fixed pitch and constant speed propeller at a constant power setting. The method which has been used is a cubic spline method for fixed pitch propellers [37]. This method allows thrust to be approximated at a given power mode as a function of airspeed. The Influence of altitude is also taken into account [38]. The air density for a certain altitude corresponds to the International Standard Atmosphere (ISA):

$$\rho = \rho_0 * (1 - \frac{H}{44308})^{4.256} \tag{3.61}$$

where $\rho_0 = 1.225 Kg/m^3$.

The thrust factor for various altitudes is:

$$T_\rho = 1 + 0.132 * \frac{\rho}{\rho_0} - 0.132 \tag{3.62}$$

Thus, the estimated thrust is:

$$T_{V_0} = (A.V_0^3 + B.V_0^2 + C.V_0 + D) * T_\rho \tag{3.63}$$

Where the constants A, B, C, and D are determined using the following matrix equation:

$$\begin{bmatrix} 0 & 0 & 0 & 1 \\ V_C^3 & V_C^2 & V_C & 1 \\ 3V_C^2 & 2V_C & 1 & 0 \\ V_0^3 & V_0^2 & V_0 & 1 \end{bmatrix} \begin{Bmatrix} A \\ B \\ C \\ D \end{Bmatrix} = \begin{bmatrix} T_{Static} \\ T_C \\ -\eta_C * 325.8 * P_{HP}/V_C^2 \\ T \end{bmatrix}$$

Where the airspeeds V_C and V_0 should in true airspeed unit (KTAS) for a right solution. The constants A, B, C, and D can obtain by solve linear system $A * X = B$.

Carson suggests that flying at a speed of about 32% higher than the best glide airspeed is more advantageous. Carson's airspeed can be considered the "fastest efficient airspeed" to fly and defines as aircraft cruise speed V_C [39].

The required thrust is equal to the thrust corresponding to the aircraft drag force. Thus, the required thrust equation:

$$D_{AC} = D_{0,AC} + D_{i,AC} \tag{3.64}$$

Where $D_{0,AC}$ is the aircraft zero-lift drag, as previously mentioned. The induced drag of the aircraft is:

$$D_{i,AC} = \frac{(W * g)^2}{(100 * q * \pi * e)} \tag{3.65}$$

To detected the maximum lift-to-drag ratio speed of the aircraft $V_{L/D_{max}}$ needs finding maximum lift/drag ratio, where $V_{L/D_{max}}$ correspond to max lift/drag ratio $L/D_{max_{AC}}$.

$$L/D_{max_{AC}} = \frac{C_{L_{max_{AC}}}}{C_{D_{max_{AC}}}} \tag{3.66}$$

and

$$L/D_{AC} = \frac{C_{L_{AC}}}{C_{D_{AC}}} \tag{3.67}$$

Lift and drag coefficients of the aircraft are needed to calculate the lift/drag ratio.

$$C_{L_{AC}} = \frac{W * g}{S * q} \tag{3.68}$$

Total drag coefficient includes zero-lift and induce drags.

$$C_{D_{AC}} = C_{D_{0_{AC}}} + C_{D_{i_{AC}}} \tag{3.69}$$

$$C_{D_{i_{AC}}} = C_{L_{AC}}^2 * K \tag{3.70}$$

$$K = \frac{1}{\pi * AR * e} \tag{3.71}$$

Where $C_{D_{0_{AC}}} = 0.026$ & e= 0.8 for for small single engine aircraft [38].

The minimum flight speed or stall speed of the aircraft is:

$$V_s = \sqrt{\frac{2 * W * g}{\rho * S * C_{L_{max_{AC}}}}} \tag{3.72}$$

3.12.1 Required and available power

The power required to move the aircraft under a specific speed at a certain altitude is determined by the propeller. Power required is estimated by multiplying required thrust by the airspeed:

$$P_{req} = T_{req} * V_0 \tag{3.73}$$

where $T_{req} = D_{AC}$

Power available is determined in the same way of power required and is given by:

$$P_{av} = T_{av} * V_0 \tag{3.74}$$

where $T_{av} = T_{V_0}$

Excess power which is:

$$P_{ex} = P_{av} - P_{req} \tag{3.75}$$

3.12.2 Rate of Climb

The rate-of-climb (ROC) determine the rate at which the airplane increases its altitude. ROC can be calculated as follows [37]:

$$ROC = \frac{T_{V_0} * V_0 - D_{AC} * V_0}{W * g} = \frac{P_{av} - P_{req}}{W * g} \tag{3.76}$$

Flight speed of maximum ROC V_y corresponds to the maximum difference between the available and required power [40]:

$$P_{av} - P_{req} = max; V = V_y \tag{3.77}$$

Consequently, maximum ROC is achieved at V_y:

$$ROC_{max} = \frac{P_{av}(V_y) - P_{req}(V_y)}{W * g} \tag{3.78}$$

3.12.3 Flight range

Electric airplanes differ from combustion engine aircraft in that their weight does not change with the range. For that, the endurance time of the motor is total battery energy over the power required [37]:

$$t_{TOT} = \frac{E_{TOT}}{(P_{req}/\eta_P)} \tag{3.79}$$

Range of flight:

$$R = V_0 * t_{TOT} \tag{3.80}$$

Chapter 4

Propeller design specifications

4.1 Pipistrel Alpha Electro specifications

Pipistrel Alpha Electro airplane and it's propeller have been designed with specifications presented in Tables 4.1 and 4.2. These specifications were considered in the design of the new propeller [41, 42].

Table 4.1: Pipistrel Alpha Electro specifications.

ELECTRO MOTOR (max)	60 kW
Maximum continuous power	50 kW
RPM	2100 to 2400
Battery capacity (total)	21.0 kWh
Maximum weight takeoff (MTOM)	550 kg
Wing span	10.5 m
Wing surface	9.51 m^2
Aspect ratio	11.8
Lift drag ratio	17

Table 4.2: Pipistrel Alpha Electro performance.

Typical cruise speed at MTOM	85 kts (157 km/h)
Stall speed flaps full at MTOM	35 kts (64 km/h)
Max. climb speed	76 kts (140 km/h)
Max. climb rate at MTOM (sea level)	6.1 m/s
Absolute ceiling at MTOM	3900 m
Max. speed at MTOM (sea level)	108 kts (201 km/h)
Standard range at cruise 85 kts	65 NM (120 km)
Propeller – fixed pitch	Two blades, diameter (1.8 m)
Or propeller – fixed pitch	Three blades, diameter (1.64 m)

4.2 Proposed flight

Conventional aircraft flight can be divided into four major phases: take-off, climbing, cruising, and landing. Thus, the proposed flight phases are:

1- Take-off.

2- Climb at maximum power at a speed of the maximum Rate of Climb V_y till 3000 m.

3- Cruising for 30 min at cruise speed V_C.

4- Landing.

Flight time is selected based on the average time of training flight and the battery capacity of the airplane. The climb and cruise phases consume more than 95% of the total energy consumption. Therefore, take-off and landing phases are not considered in the calculation [43].

4.3 New propeller specifications

The new Pipistrel Alpha Electro propeller is a fixed pitch propeller and the input specifications for the design are detailed in Tables 4.3 and 4.4.

Table 4.3: Input data for the new propeller design.

ELECTRO MOTOR (max)	60 kW
RPM	2400
Maximum weight takeoff (MTOM)	550 kg
Propeller diameter	1.8 m
Number of blades	2
Propeller airfoil	Clark Y
Blade element section (dr)	0.1 m

Table 4.4: Propeller blade geometry dimensions.

r (m)	**0.3**	**0.4**	**0.5**	**0.6**	**0.7**	**0.8**	**0.85**
Chord (m)	0.153	0.145	0.135	0.123	0.11	0.095	0.085
Thickness (m)	0.027	0.02	0.016	0.0134	0.011	0.009	0.008

4.4 Propeller of RAF 6 airfoil

The use of the RAF 6 airfoil in the propeller design and its performance has been investigated and compare with that of Clark Y airfoil. The difference of calculation between RAF 6 and Clark Y airfoils is in computing zero-lift angle α_0, which is explained in section 3.6.

4.5 Fixed and variable pitch propeller

For a fixed pitch propeller, the RPM and airspeed is controled by throttle. High propeller pitch position (coarse) is usually used for all-round performance due to high efficiency during cruise flight. High propeller pitch reduces blade angle drag and RPM [44]. In contrast, a variable pitch propeller allows the propeller to maintain the ideal blade setting for the flight condition by adjusting the pitch propeller between low pitch (fine) and coarse position based on the altitude, engine RPM, and other parameters.

Limitation of electric aircraft by its construction and weight leads to using fixed pitch propellers [7]. Also, limited torque is another reason for a fixed pitch propeller [45]. Therefore, a comparison between fixed and variable pitch propellers is investigated in this report.

One of the issues of fixed pitch propeller is the stall and collapse of the air-stream over the propeller blade at low speed aircraft, which is caused by a high lift coefficient. Where the blade lift coefficient exceed the max lift coefficient of the blade $C_L > C_{L_{max}}$. The simplest solution for this issue by using a variable pitch propeller, but this is expensive, particularly for light aircraft.

Applying the design method on a variable pitch propeller differs from a fixed pitch propeller when considering the operating points as design points in order to calculate the optimum blade angle for each flight condition. In other words, using the altitude, sound speed, and the density of the operation point in the calculation from section 3.5 till 3.10.

4.6 Influence of blades number

Increasing the number of blades will increase the generated torque, which does not allow the engine to run at the original RPM, generating less thrust. The easiest way to solve this issue is to reduce the diameter of the propeller. Furthermore, increasing the number of blades reduces the propeller noise and blade vibration. This attribute to less tip speed of the propeller and leads to smaller pressure pulses per revolution. The proper diameter of a propeller by increasing the number of blades with maintaining the same power consumption can be calculated by the formula [46]:

$$D_{new} = D_{old} * (\frac{Z_{old}}{Z_{new}})^{1/4} \tag{4.1}$$

As a result, D_{new} using the above method suggests diameters 90% and 84% of the original diameter for 3 and 4 blades, respectively.

Chapter 5

Results and discussion

The propellers performances was analyzed using Glauert's theory [10] with Bratt improvements [32]. To verify the capability of the method, three operations points were calculated, which are the design point, the cruise phase, and the static phase.

5.1 Design point performance

The selected values in Table 4.3 of diameter, forward speed, and RPM show an optimum value of the advance ratio, which approximately corresponds to the highest efficiency, as shown in Figure 5.1. That provides a good indication of the initial performance of the propeller.

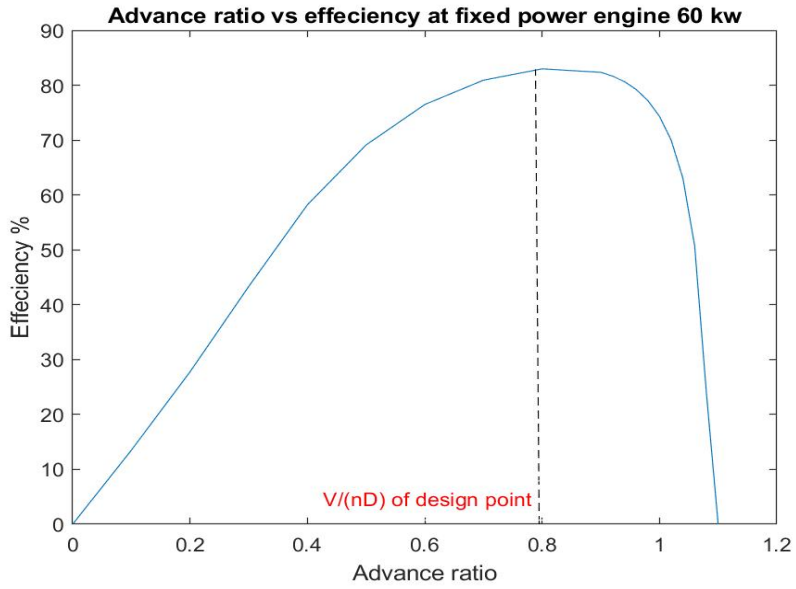

Figure 5.1: Efficiency variation versus advance ratio at full engine power.

Propeller specifications at the design point are displayed in Table 5.1. It is observed that the aircraft speed is faster than Pipistrel Alpha Electro speed by 5.2 km/h. The tip velocity of the propeller equals 0.66 Mach, that leads to the ability to use a metal propeller [37]. The propeller efficiency η occurs in the range of a good performance light aircraft efficiency, which is from 0.8 to 0.85 [32].

Table 5.1: Propeller specifications for the design point.

V_0	57 m/s (205.2 km/h)	V_s	18 m/s (64.8 km/h)
Ω	251.3 rad/sec	Ω.r	226.2 m/s
Q	238.7 N.m	Q_0	185.9 N
T	859.3 N	η	0.832
C_P	0.04	C_T	0.042
C_Q	0.0064	CG	0.63

Table 5.2 illustrates the result of the design parameters and angles for each blade element along the propeller blade. It can be seen that V_1>V_0 condition achieved for all blade elements. Increasing the slipstream speed V_1 causes an increase in the drag of the aircraft body, and V_1 can be reduced by reducing the blade angle. The *dQ* distribution considered the largest value of *Q* close to *CG* , where high *dQ* at the blade tip causes a stall at the inner part of the blade at zero and low speed.

High importance parameters in the design are the distribution *dT* of the load and blade angle β. The choice of chord and thickness has secondary importance for the aerodynamics loads [32] which is effect the value of C_L. On the other hand, it is an extreme matter of the stress loads for the blades. Thrust and torque distribution and pitch blade angles distribution are presented in Figures 5.2 and 5.3. The area below the *dQ* curve must equal Q_0, and the *CG* must be located in a balance point for the engine torque and the aerodynamic loads.

Table 5.2: Analyzing the blade elements for the design point.

r (m)	**0.3**	**0.4**	**0.5**	**0.6**	**0.7**	**0.8**	**0.85**
dQ	16	25	31	34	35.4	33	30
dT	18.34	38.98	59.84	77.80	93.30	97.33	91.78
V_1	58.36	59.23	60.18	60.86	61.52	62.32	63.33
Mach number	0.27	0.34	0.40	0.47	0.54	0.61	0.65
C_L	0.2784	0.383	0.422	0.429	0.430	0.402	0.376
$C_{L_{max}}$	1.482	1.450	1.396	1.319	1.217	1.091	1.018
C_{D_0}	0.0144	0.0123	0.0112	0.0106	0.0101	0.0096	0.0095
K	1.00	0.96	0.81	0.71	0.62	0.48	0.35
α	2.51	3.45	3.80	3.86	3.87	3.62	3.39
α_0	8.06	6.52	5.74	5.36	5.00	4.79	4.76
α_i	1.05	1.29	1.47	1.48	1.49	1.53	1.71
ϕ_i	38.14	30.84	25.87	22.19	19.44	17.36	16.65
ϕ	37.09	29.55	24.40	20.71	17.95	15.83	14.94
β_0	40.64	34.29	29.66	26.05	23.30	20.97	20.04

Figure 5.4 shows the drag and thrust curves over the speed for the setting power. Intersection points give the minimum and maximum speeds for the aircraft. The highest thrust also is an indication for the propeller blades stall. Figure 5.5 displays the key airspeeds for the aircraft. It is crucial that the minimum speed of the aircraft is smaller than its stall speed to maintain the aircraft under control during stall. maximum climb speed V_y is always located at the peak of the excess power.

Propeller efficiency plotted via using the cubic spline method, as shown in Figure 5.6. It is showing the standard shape for propeller efficiency for a constant-speed, and the cruise speed located at the highest efficiency. Additionally, the propeller efficiency is high at high aircraft speed. On the contrary, the thrust is high at low aircraft speed.

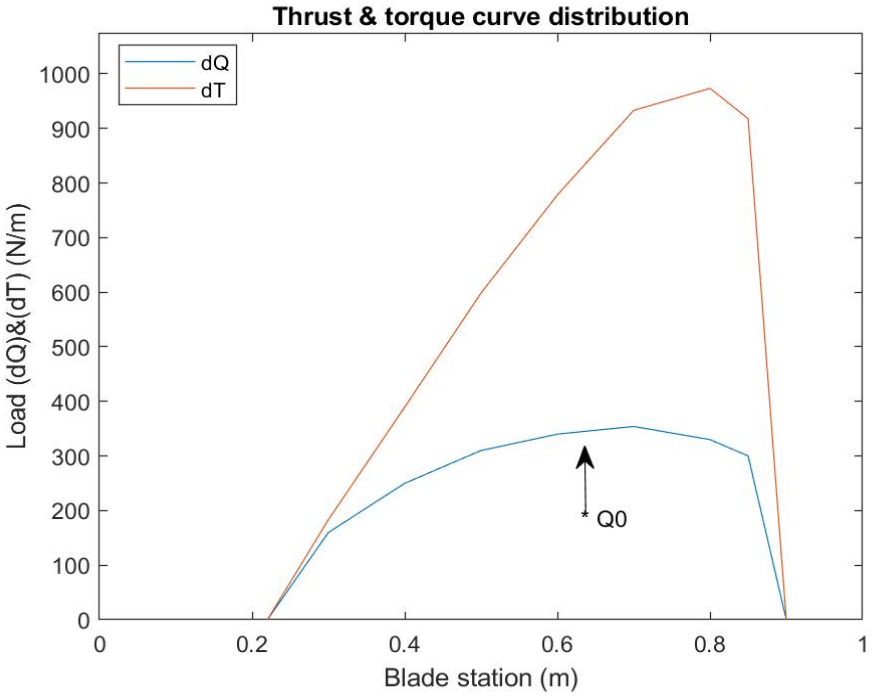

Figure 5.2: Thrust and torque distribution at the design point.

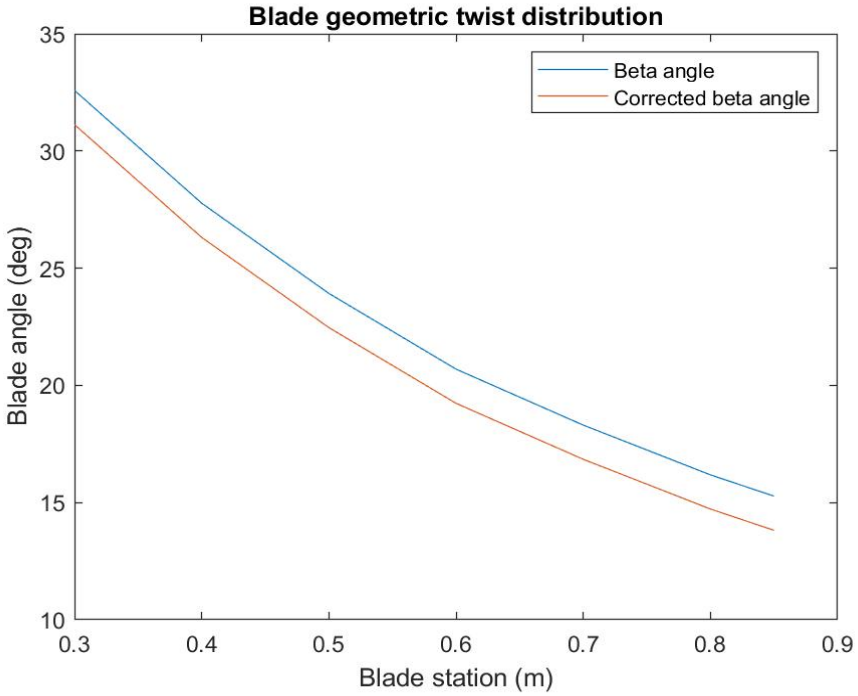

Figure 5.3: Beta and corrected beta angle distribution along the blade.

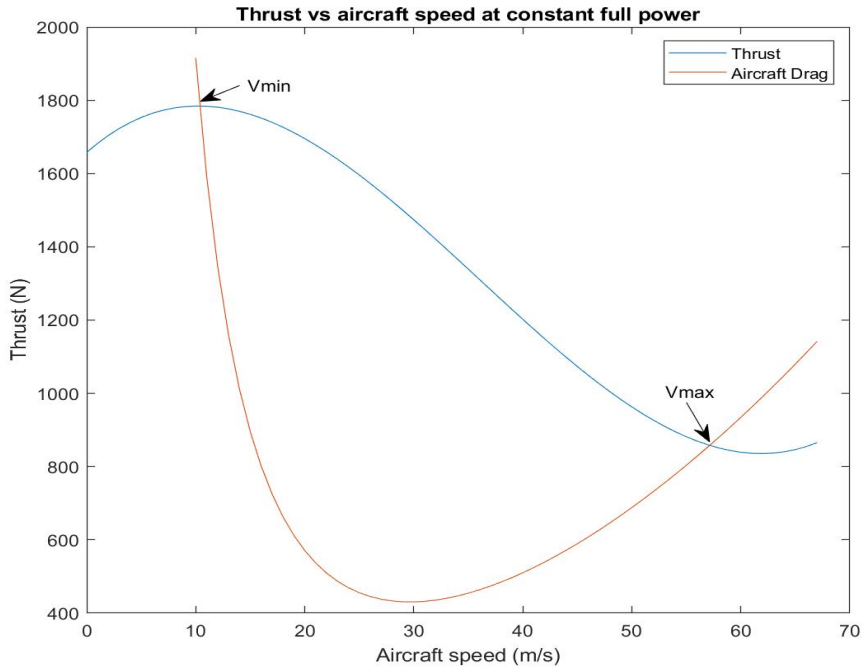

Figure 5.4: Thrust at constant full power versus aircraft speed.

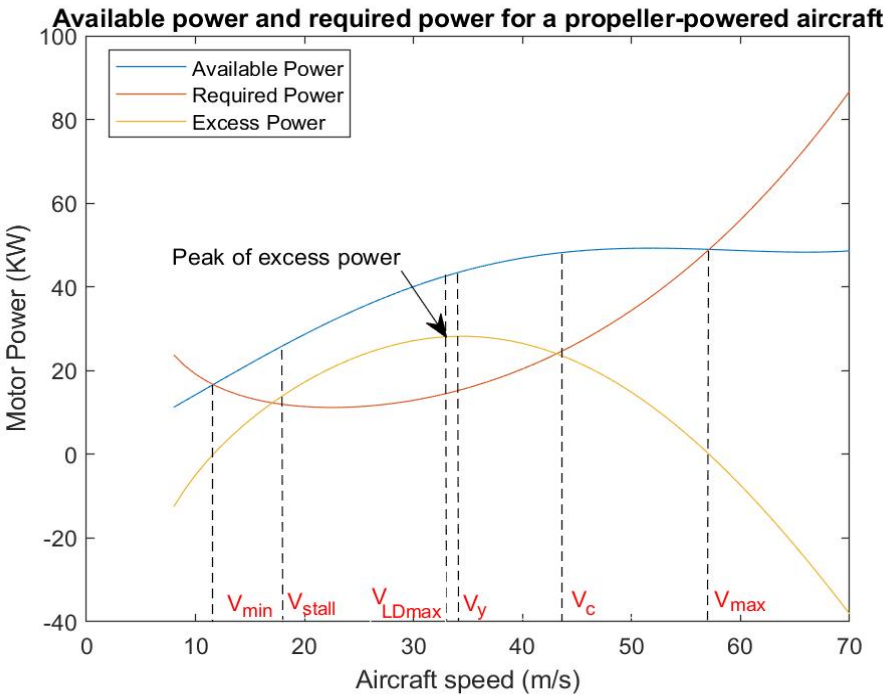

Figure 5.5: Engine power versus aircraft speed.

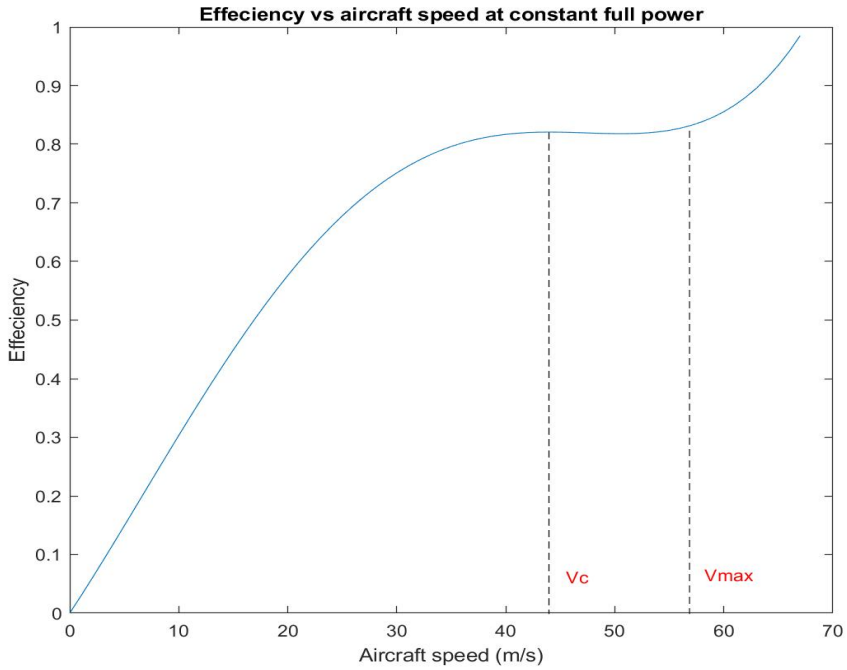

Figure 5.6: Propeller efficiency at constant full power versus aircraft speed.

Figures 5.7 and 5.8 are elaborated $V_{L/D_{max}}$ and V_y speeds that explained in Figure 5.5. Figure 5.7 shows the lift to drag ratio curve at sea level where maximum lift to drag ratio is 16.9 and corresponding $V_{L/D_{max}}$. Figure 5.8 shows the Rate of Climb curve at sea level, where V_y is 32 m/s (115.2 km/h) and ROC_{max} is 5.86 m/s.

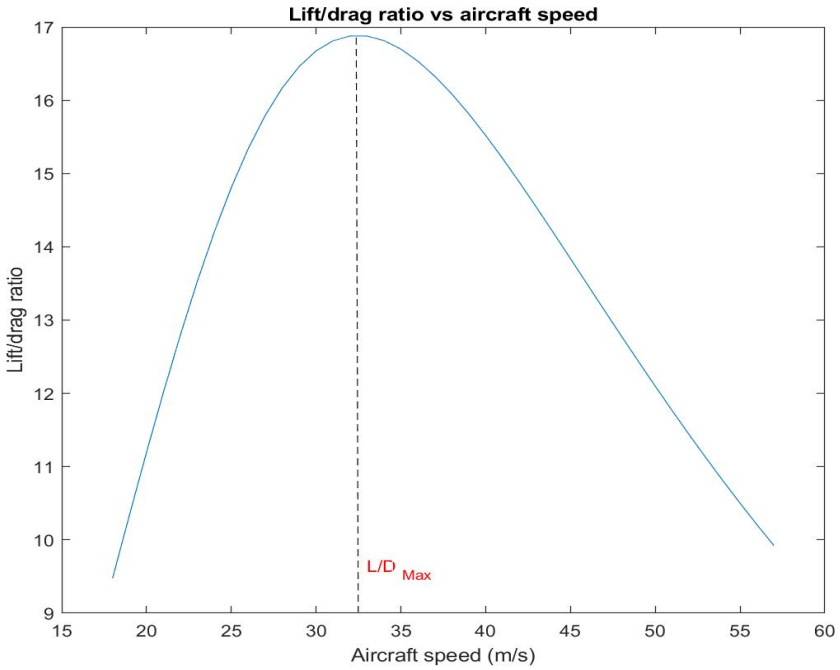

Figure 5.7: Lift drag ratio versus aircraft speed at sea level.

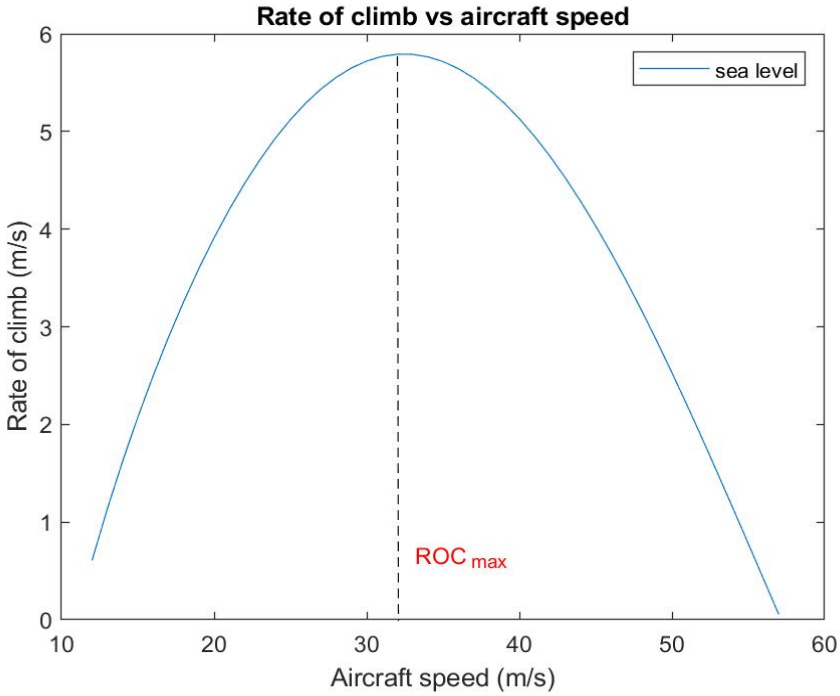

Figure 5.8: Rate of Climb of the aircraft at sea level.

Static thrust ($V_0 = 0$) using the three methods mentioned in the method chapter at sea level is presented in Table 5.3.

Table 5.3: Propeller performance for static phase at sea level.

ELECTRO MOTOR	45 kW
RPM	1800
Bratt method thrust	1364.7 N
Bendemann formula thrust	1368.7 N
Thrust by thrust coefficient measured	1388.8 N
Figure of merit	0.51

5.2 Cruise phase performance

Propeller specifications for the cruise phase at sea level are shown in Table 5.4. The aircraft speed has the same cruise speed as Pipistrel Alpha Electro by applying Carson's suggestion [39]. However, the motor produces less than 50% of the maximum power. And when the aircraft speed V_0 is reduced, RPM needs to be reduced to have a balanced torque between the engine and the propeller.

Table 5.4: Propeller specifications for the cruise phase at sea level.

V_0	43.5 m/s (157 Km/h)	RPM	1875
P	29.05 kW	Range at V_c	62.3 NM (115 km)
Ω	196.3 rad/sec	Ω.r	176.7 m/s
Q	147 N.m	Q_0	118.9 N
T	563.5 N	η	0.86
C_P	0.0403	C_T	0.045
C_Q	0.0065	J	0.773

Table 5.5 illustrates the result of the design parameters and angles of each blade element *dr* for the cruise phase. The lift coefficient became higher than at the maximum

speed because of the low V_0 due to a high AOA. It is observed that *dQ* and *dT* distributions are lower than *dQ* and *dT* at the design point, which can be attributed to the low thrust generated, as shown in Figure 5.9.

Table 5.5: Analyzing the blade elements for the cruise phase.

r (m)	**0.3**	**0.4**	**0.5**	**0.6**	**0.7**	**0.8**	**0.85**
dQ	11	16.6	20.2	21.7	22.6	21.1	19
dT	13	26.47	39.78	50.62	60.68	63.36	59.14
V_1	44.77	45.77	46.23	46.75	47.29	47.95	48.77
Mach number	0.22	0.26	0.32	0.37	0.42	0.48	0.51
C_L	0.333	0.430	0.46	0.459	0.458	0.428	0.40
$C_{L_{max}}$	1.495	1.486	1.464	1.429	1.378	1.312	1.273
C_{D_0}	0.0145	0.0124	0.0113	0.0107	0.0102	0.0097	0.0096
K	1.00	0.96	0.81	0.72	0.63	0.48	0.35
α	2.97	3.85	4.15	4.12	4.11	3.85	3.59
α_i	1.26	1.46	1.61	1.60	1.59	1.64	1.83
ϕ_i	37.70	30.43	25.51	21.86	19.16	17.11	16.43
ϕ	36.45	28.98	23.90	20.27	17.56	15.48	14.61
β_0	40.67	34.29	29.66	25.99	23.27	20.97	20.02

5.3 Aircraft performance at variance altitudes

Propeller thrust characteristics at high altitudes draw the flight capability of the aircraft for the pilot. Figure 5.10 shows thrust and aircraft drag at various altitudes. It can be seen the aircraft drag raising and thrust descending with increasing the altitude. Figure 5.11 displays available, required, and excess powers at the lowest and highest altitude where if the excess power equal to zero, this is the maximum flight altitude point. The absolute ceiling at MTOM for the designed propeller is 7870 m. The efficiency of the aircraft also declines with high altitude, as presented in Figure 5.12. Flight envelope shows $V_{0_{max}}$ reduces during the altitude increase, and on the other hand, $V_{0_{min}}$ raises during the altitude increase, as shown in Figure 5.13.

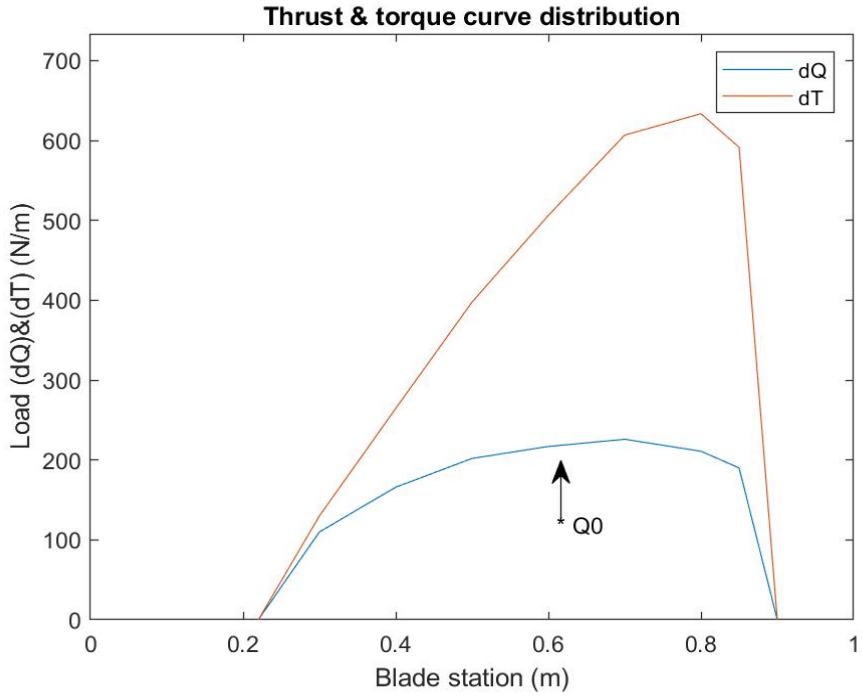

Figure 5.9: Thrust and torque distribution for cruise speed.

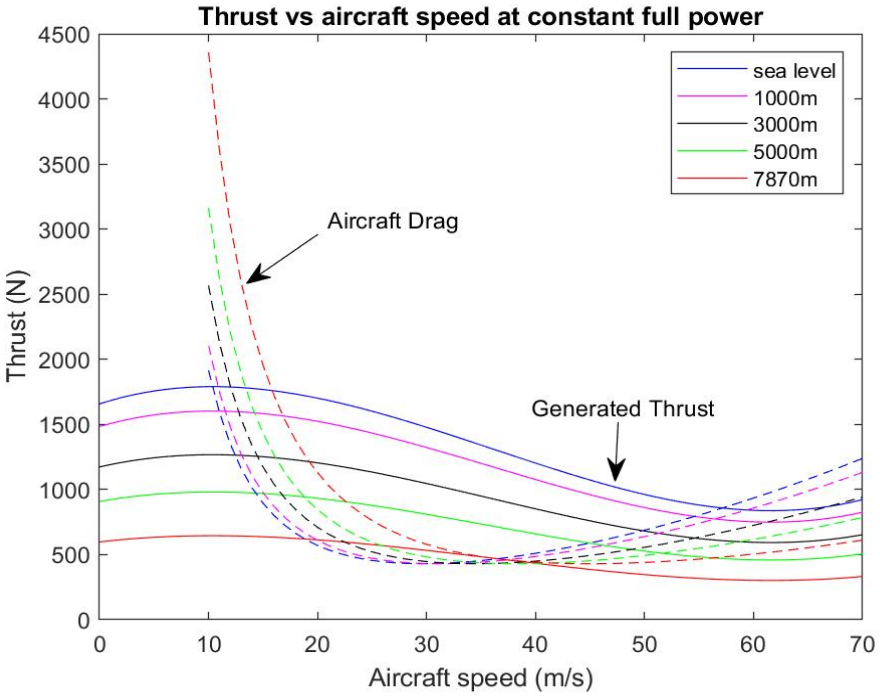

Figure 5.10: Thrust at constant full power versus aircraft speed for various altitudes.

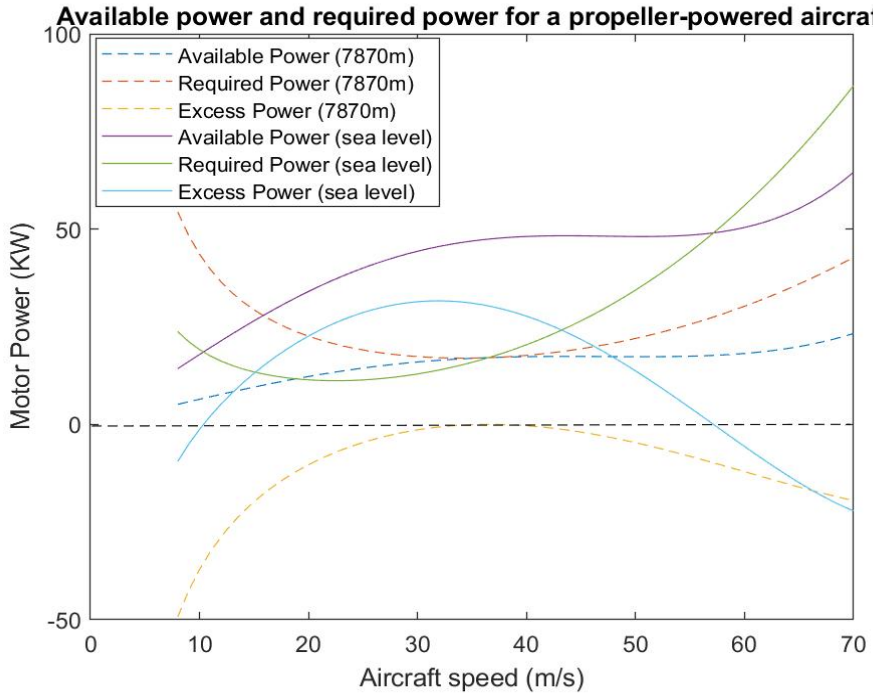

Figure 5.11: Engine power versus aircraft speed at max and min altitudes.

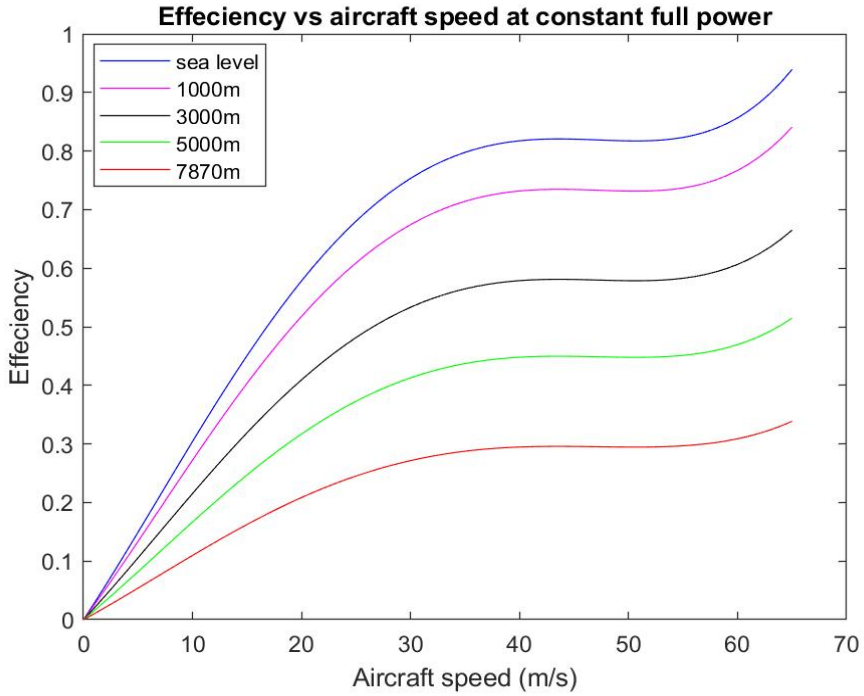

Figure 5.12: Propeller efficiency at constant full power for various altitudes.

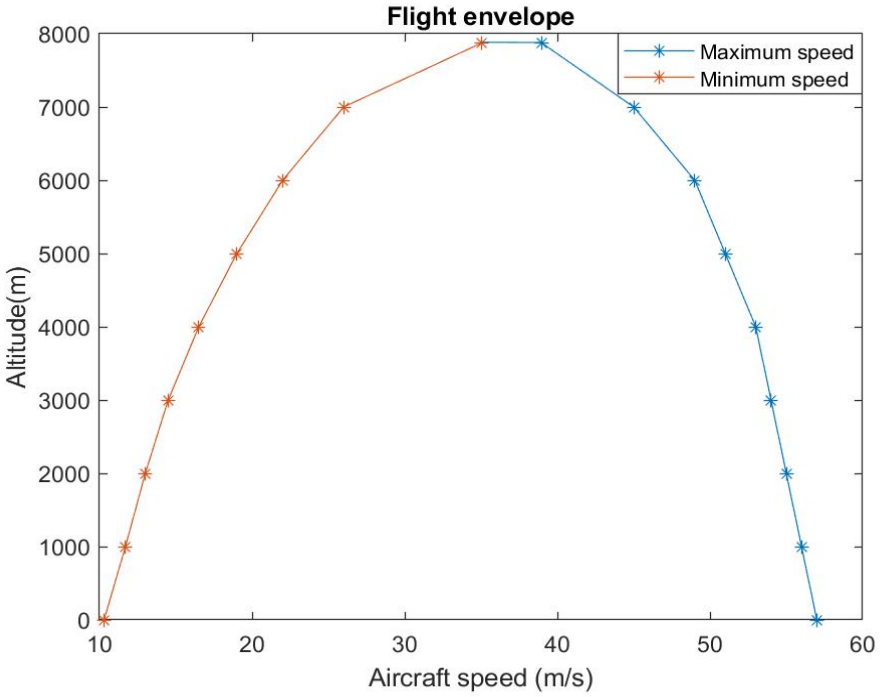

Figure 5.13: Flight envelope at constant full power.

Rate of Climb and lift drag ratio curves at various altitudes presented in Figures 5.14 and 5.15. ROC falls with high altitude as far as the maximum altitude where ROC is zero. It is observed that $V_{L/D_{max}}$ increases with rising the altitude.

5.4 RAF 6 airfoil propeller performance

In sections 5.1, 5.2 and, 5.3 the propeller was designed with Clark Y airfoil, and in this section compares the performance between Clark Y and RAF 6 airfoils propellers. RAF 6 propeller has the same blade geometry dimensions used for Clark Y propeller.

5.4.1 Design point performance

Propeller specifications at the design point are listed in Table 5.6, where a small difference in thrust and efficiency between RAF 6 and Clark Y propellers can be noticed. Distribution of dT and dQ for RAF 6 propeller is approximately identical with dT and dQ distribution of Clark Y propeller, with a small thrust increase between radius 0.5 to 0.8, as illustrated in Figure 5.16. This elaborates Clark Y propeller thrust is higher than R.A.F. 6 propeller thrust by 3.1 N at the design point.

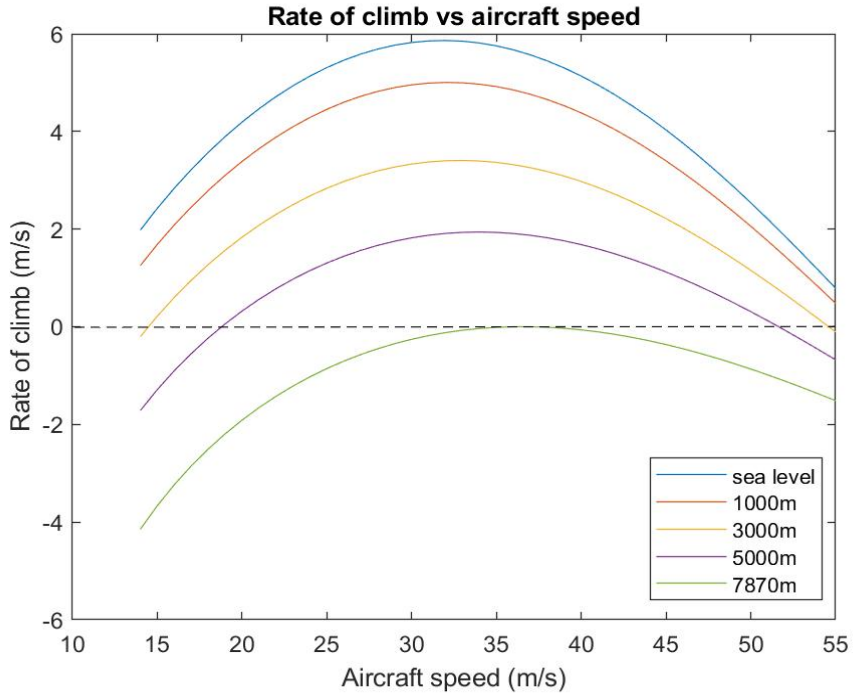

Figure 5.14: Rate of Climb of the aircraft at various altitudes.

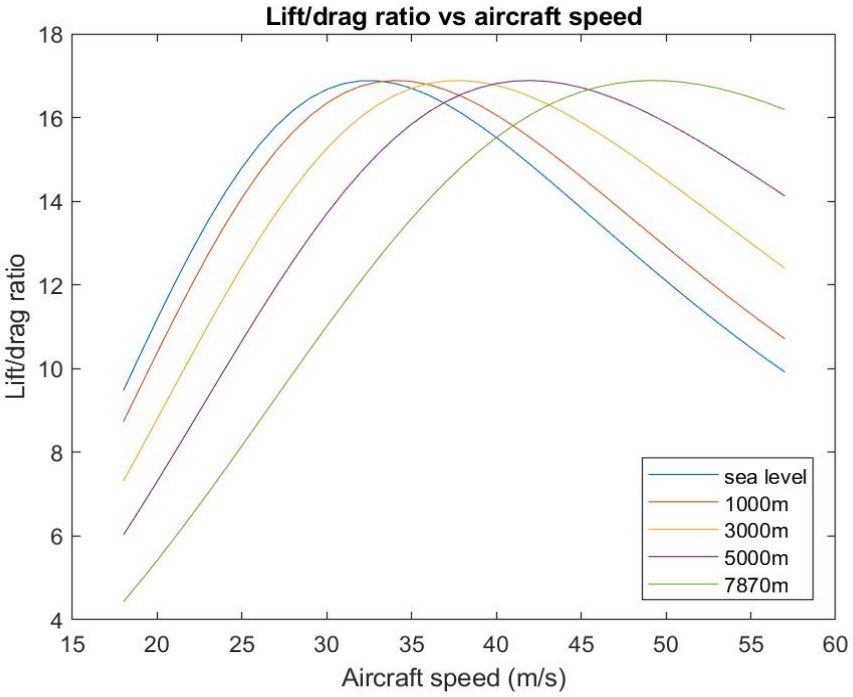

Figure 5.15: Lift drag ratio versus aircraft speed at various altitudes.

Table 5.6: Propeller specifications for RAF 6 airfoil propeller at the design point.

V_0	57 m/s (205.2 km/h)	J	0.792
Ω	251.3 rad/sec	Ω.r	226.2 m/s
Q	238.7 N.m	Q_0	185.9 N
T	856.2 N	η	0.829
C_P	0.04	C_T	0.042
C_Q	0.0064	CG	0.63

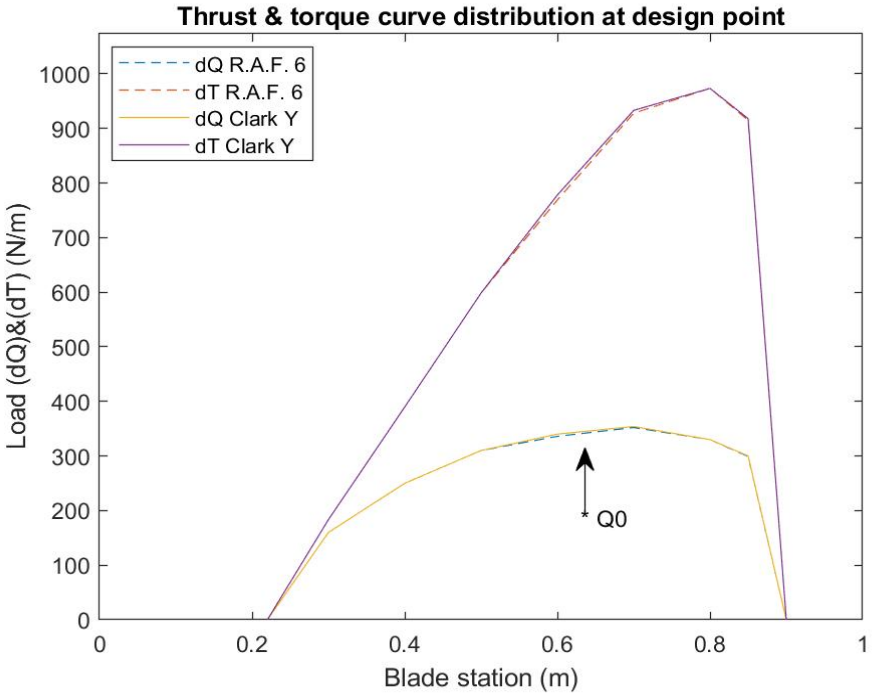

Figure 5.16: Thrust and drag distribution at maximum speed for Clark Y and RAF 6.

Figure 5.17 shows the drag and thrust curves for RAF 6 and Clark Y propellers. It is observed that RAF 6 propeller is slightly superior to Clark Y propeller at low speed flight. In contrast, Clark Y produces a little more thrust at high speed flight. Propeller efficiency has the same status as well as in Figure 5.12, where Clark Y propeller is more efficient at high speed flight and vice versa at low speed, as illustrated in Figure 5.18. Available and required power is similar for both propellers, as shown in Figure 5.19.

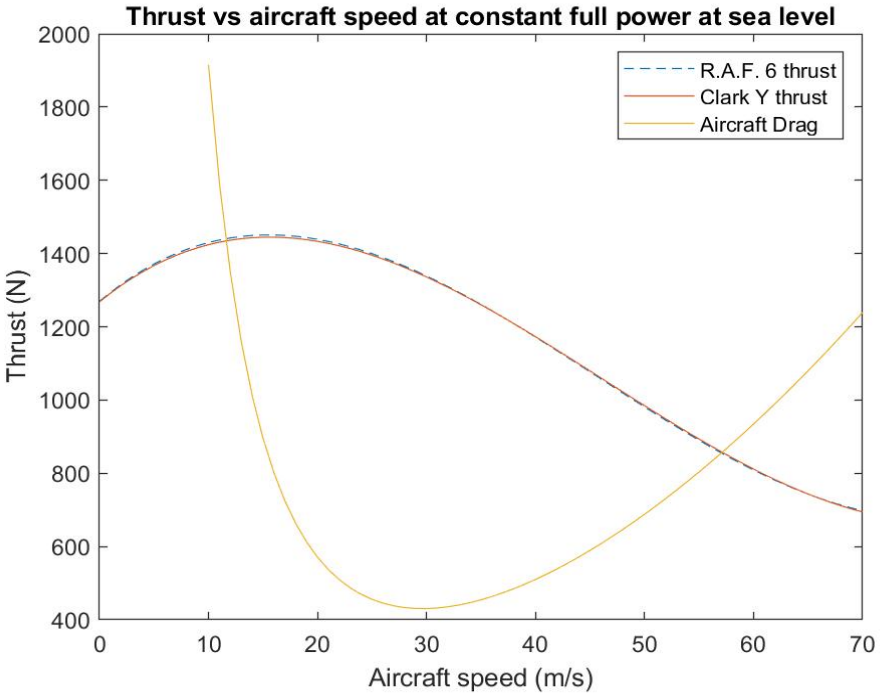

Figure 5.17: Thrust at full power versus aircraft speed for Clark Y and RAF 6.

Lift coefficient distributions at various aircraft speeds for RAF 6 and Clark Y propellers are displayed in Figure 5.20. It is noted that high C_L value for low speeds due to the high angle of attack. Also, stall speed occurs when $C_L > C_{L_{max}}$. The lift coefficient equation is less accurate at low speed aircraft and gives high values. Therefore, C_L is not calculated for the inner part of the blade from 0.3 to 0.5 m. RAF 6 propeller has a higher lift coefficient compare to Clark Y propeller. $C_{L_{max}}$ has the same value for both propellers because the same rate of Mach number for both propellers, as shown in Figure 5.21.

The angles β and α for RAF 6 and Clark Y propellers are presented in Figures 5.22 and 5.23. It is observed that RAF 6 propeller β angle is greater than Clark Y propeller β angle.

Figures 5.24 shows the Rate of Climb curve at sea level, where V_y is 32 m/s (115.2 km/h) and ROC_{max} is 5.85 m/s. Static thrust results with the three methods mentioned in chapter 3 at sea level are presented in Table 5.7.

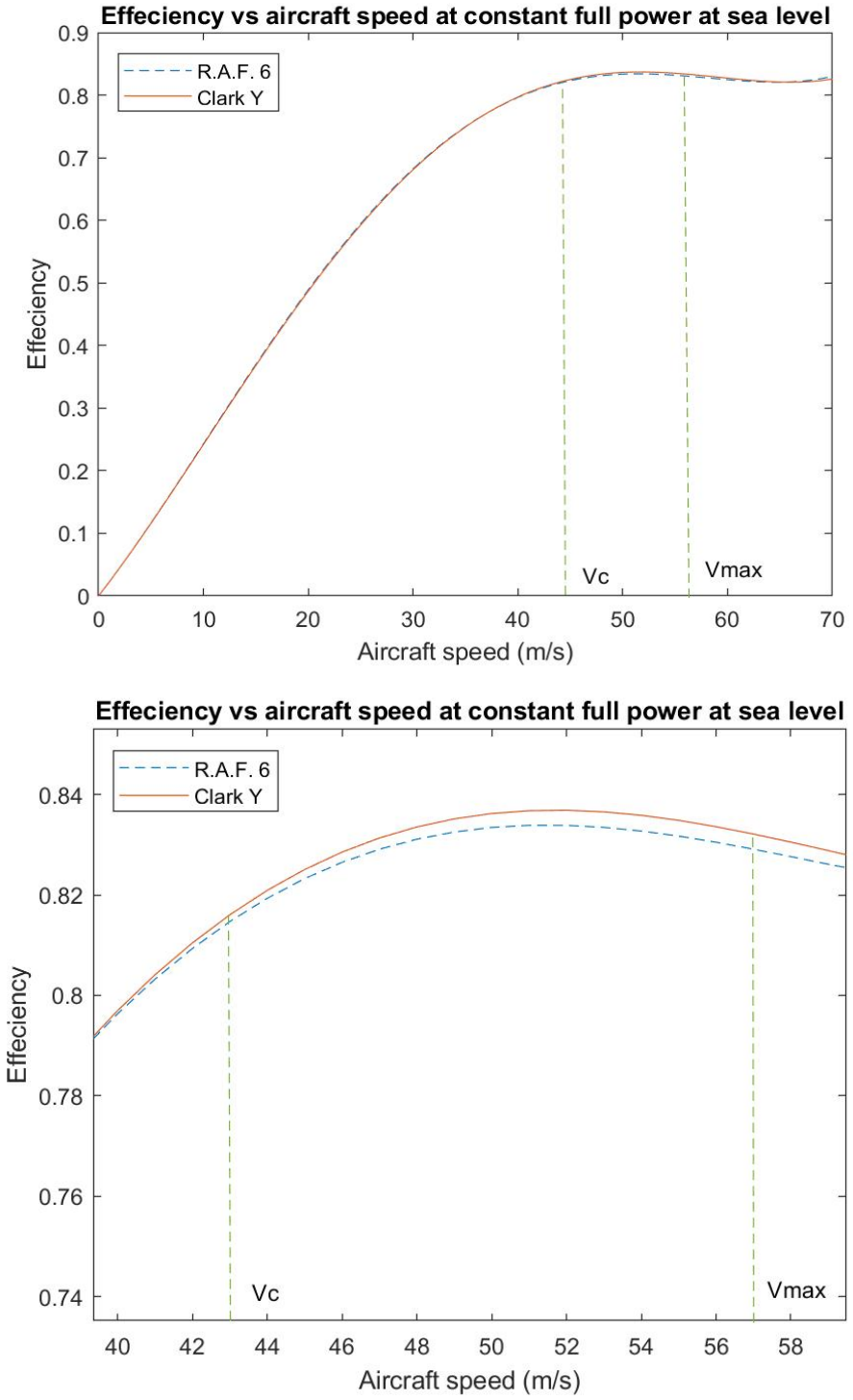

Figure 5.18: Propeller efficiency at full power for Clark Y and RAF 6.

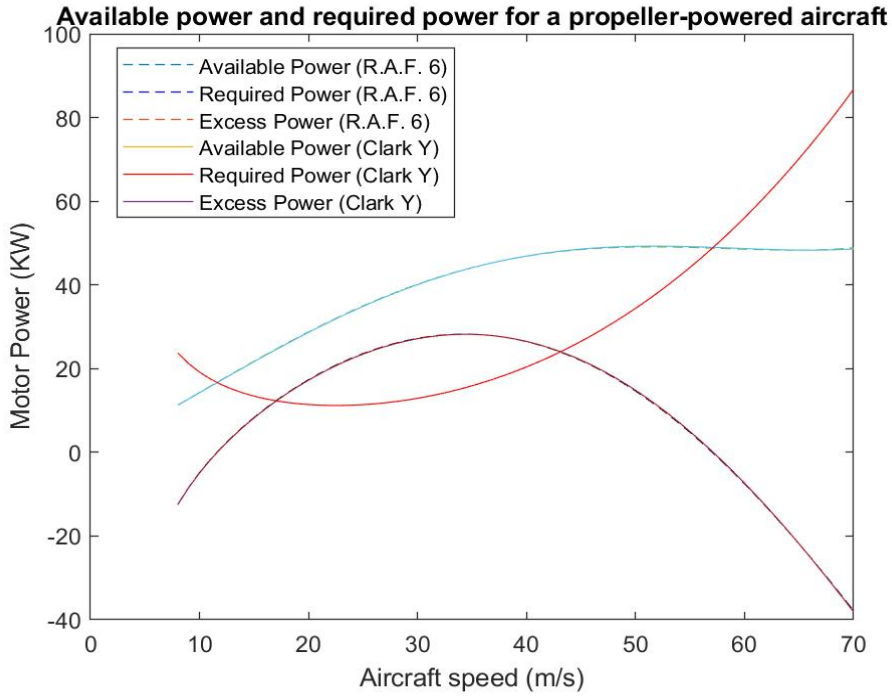

Figure 5.19: Engine power versus aircraft speed for Clark Y and RAF 6.

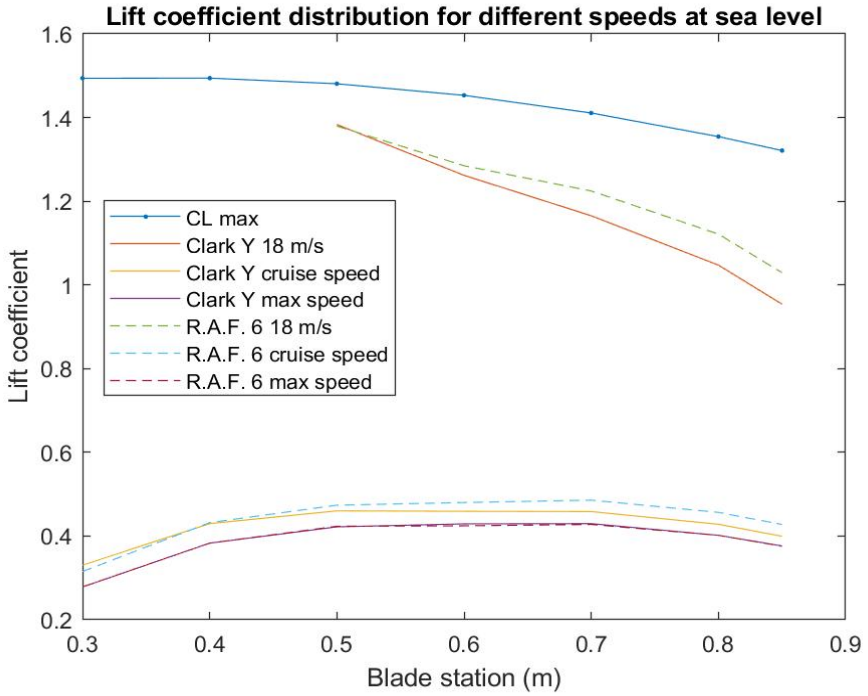

Figure 5.20: Lift coefficient distribution along the blade for Clark Y and RAF 6.

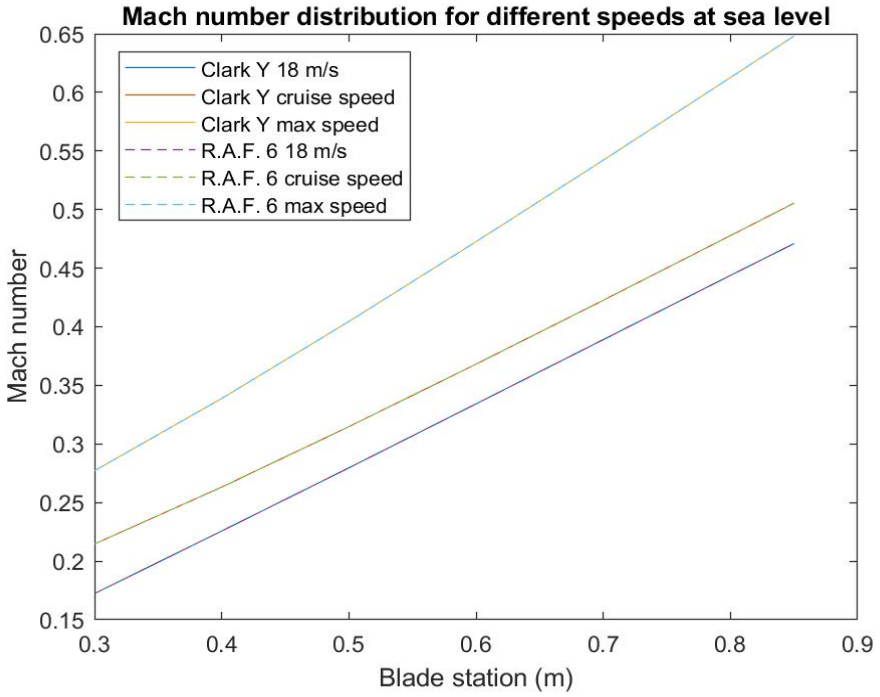

Figure 5.21: Mach number along the blade for Clark Y and RAF 6.

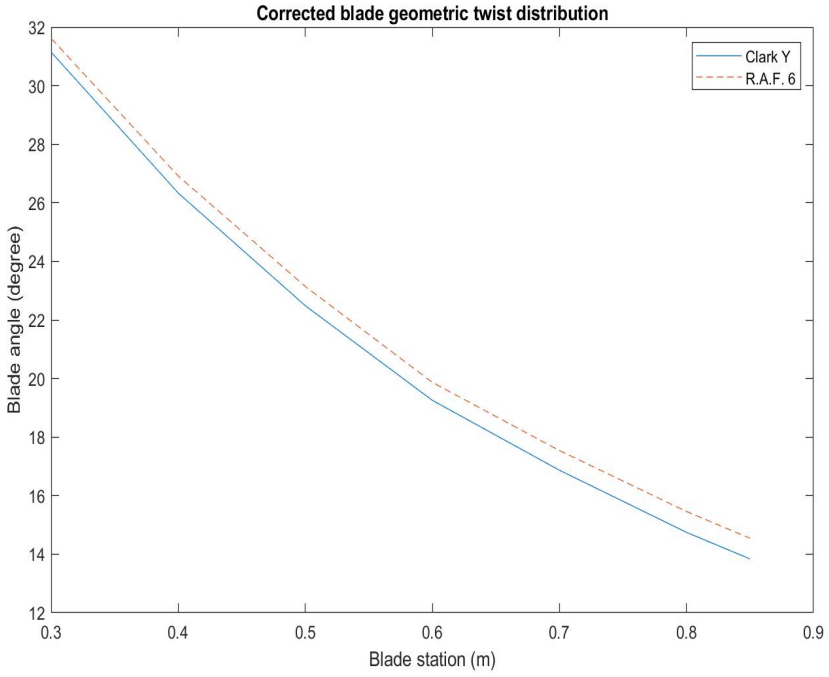

Figure 5.22: Variation of corrected blade angle for Clark Y and RAF 6 along the blade.

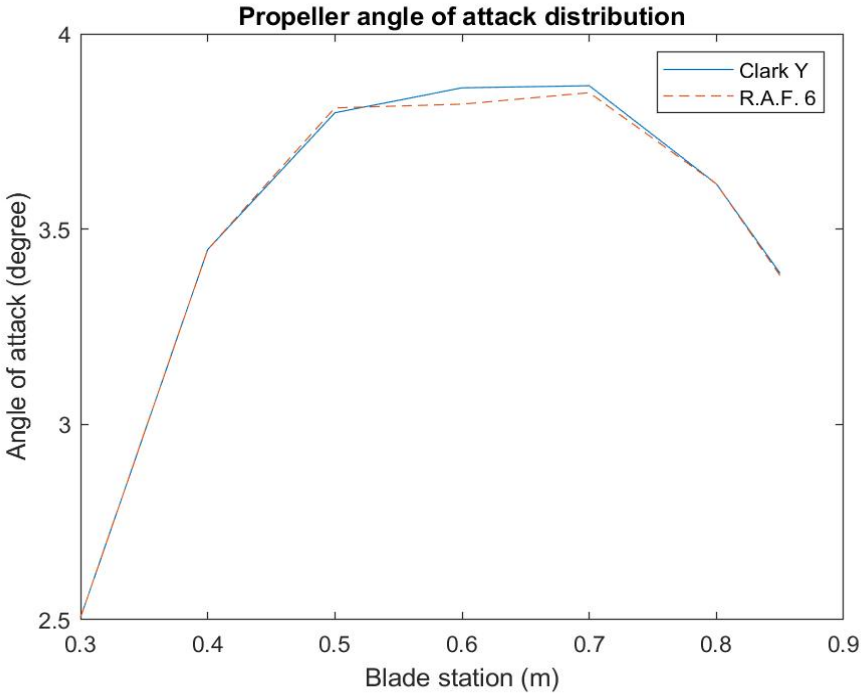

Figure 5.23: Variation of angle of attack for Clark Y and RAF 6 along the blade.

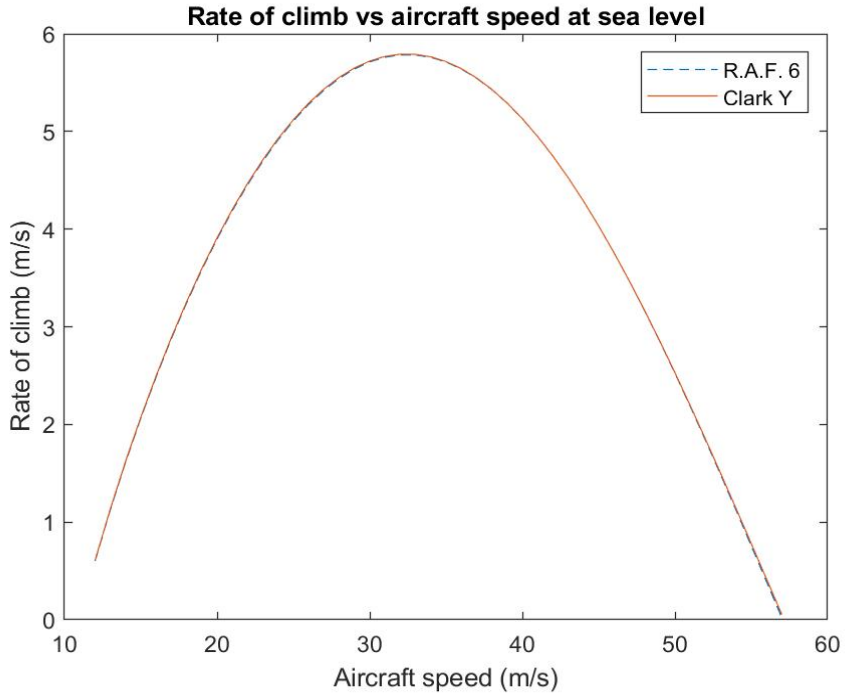

Figure 5.24: Rate of Climb of the aircraft for Clark Y and RAF 6.

Table 5.7: RAF 6 Propeller performance for static phase at sea level.

ELECTRO MOTOR	45 kW
RPM	1800
Bratt method thrust	1368.1 N
Bendemann formula thrust	1368.7 N
Thrust by thrust coefficient measured	1388.8 N
Figure of merit	0.51

5.4.2 Cruise phase performance

Propeller specifications for the cruise phase at sea level are displayed in Table 5.8. It is noted that the generated power and RPM for RAF 6 are less compare to Clark Y propeller for the same generated thrust.

Table 5.8: Propeller specifications for the cruise phase at sea level.

V_0	43.5 m/s (157 Km/h)	RPM	1832
P	28.85 kW	J	0.79
Ω	191.8 rad/sec	Ω.r	172.6 m/s
Q	150.4 N.m	Q_0	120.9 N
T	563.5 N	η	0.86
C_P	0.0403	C_T	0.045
C_Q	0.0065		

There is more contrast between the two propellers *dT* and *dQ* distribution compare to design point *dT* and *dQ* distribution, as shown in Figure 5.25. Furthermore, *dQ* of RAF 6 is larger than *dQ* of Clark Y.

5.4.3 RAF 6 airfoil propeller performance at various altitudes

The absolute ceiling at MTOM is 7860 m, which is 10 m less than that obtained using the Clark Y propeller. Specifications Figures of RAF 6 airfoil propeller performance at various altitudes are available in the Appendix.

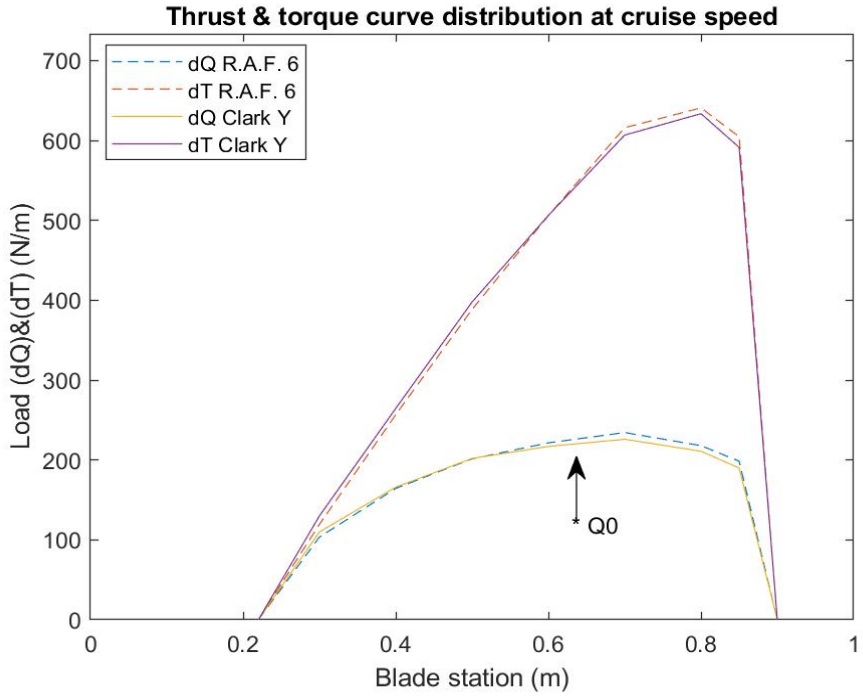

Figure 5.25: Thrust and drag distribution at cruise speed for Clark Y and RAF 6.

5.5 Consumed power of the proposed flight

The consumed power has been computed for the Clark Y airfoil propeller that used variable and fixed pitch. The comparison between variable and fixed pitch propeller was carried out for the cruise phase only at 3000 m altitude, due to the largest amount of energy being consumed during the flight. Table 5.9 shown the expended energy of the entire proposed flight for the fixed pitch propeller. The expended energy of the cruise phase for variable and fixed pitch propeller is presented in Table 5.10. It can be noted that the variable pitch propeller saved 0.07 kW through the cruise flight compared to the fixed pitch propeller for the same flight range. This improvement is limited in comparison with the change from fixed pitch to variable pitch propeller. The climb phase for the fixed pitch propeller is shown in Table 5.11.

5.6 Influence of blade numbers

In order to have well-defined comparison between the difference of blades number, all therewith parameters are fixed (RPM, blade chord, blade thickness, motor power, MTOT). Table 5.12 presents the specifications for 2, 3, and 4 blades propellers at the design point. It is observed that the propeller with 3 blades has the highest thrust and efficiency. Also,

Table 5.9: Consumed power of fixed pitch propeller for the proposed flight.

Battery capacity, total	21.0 kWh
Climb consumed power	3.93 kW
Percentage of power consumed (climb)	18.7 %
Cruise consumed power	12.5 kW
Percentage of power consumed (cruise)	59.5 %
Total consumed power	16.43 kW
Total percentage of power consumed	78.2 %
Remaining battery energy	4.57 kW

Table 5.10: Consumed power of variable and fixed pitch propeller for the cruise phase.

	Fixed Pitch Propeller	**Variable Pitch Propeller**
RPM	1930	1930
Consumed power	12.5 kW	12.43 kW
Average cruise speed	43.5 m/s	43.5 m/s
Propeller cruise efficiency	0.85	0.854
Cruise time	30 min	30 min
Range of cruise phase	42.3 NM (78.3 km)	42.3 NM (78.3 km)

Table 5.11: Consumed power of fixed pitch propeller for the climb phase.

RPM	2400
Consumed power	3.93 kW
Average cruise speed	33 m/s
Propeller climb efficiency	0.65
Climb time	11 min
Horizontal range of climb phase	11.8 NM (21.8 km)

this leads to that less number of blades does not signify the propeller is more efficient. Moreover, the advance ratio is increasing with more propeller blades, is also shown by Lieser [25].

Table 5.12: Propeller specifications of various number of blades at the design point.

	2 blades	**3 blades**	**4 blades**
Diameter	1.8 m	1.63 m	1.51 m
dr	0.1 m	0.09 m	0.084 m
V_0	57 m/s (205.2 Km/h)	57.7 m/s (207.7 km/h)	57.3 m/s (206.3 km/h)
Ω	251.3 rad/sec	251.3 rad/sec	251.3 rad/sec
Ω.r	226.2 m/s	204.4 m/s	190.2 m/s
Q	238.7 N.m	238.7 N.m	238.7 N.m
Q_0	185.9 N	137.1 N	110.5 N
T	859.3 N	877.4 N	869 N
η	0.832	0.85	0.841
C_P	0.04	0.066	0.095
C_T	0.042	0.064	0.085
C_Q	0.0064	0.0107	0.015
J	0.792	0.876	0.941

The β and α angles for 2, 3, and 4 blades propellers are presented in Figures 5.26 and 5.27. It is noticed that the upturn blade angle comes with increasing the number of blades and vice versa for the angle of attack. The reason behind that is the reduction in diameter, also β increasing by increases the thrust and α decreasing by increasing the forward velocity. Figures 5.28 and 5.29 show thrust and aircraft drag for 2, 3, and 4 blades and the corresponding propeller efficiency. Figure 5.30 illustrates the Rate of Climb curve at sea level for the different number of blades. The maximum climb speed is 32 m/s (115.2 km/h) and the maximum climb rates are 5.86 m/s, 5.89 m/s, and 5.85 m/s for 2, 3, and 4 blades respectively.

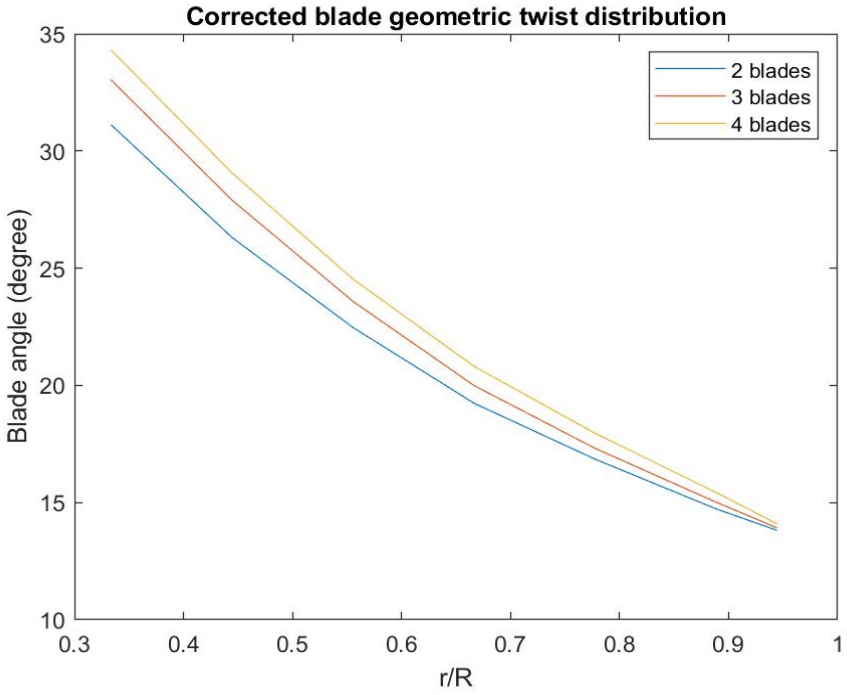

Figure 5.26: Variation of corrected blade angle for different number of blades.

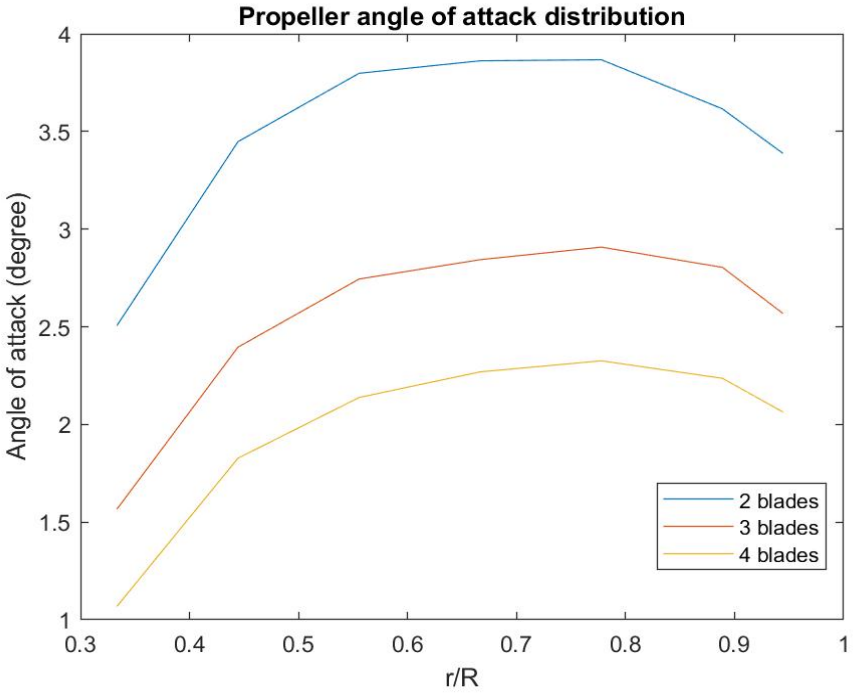

Figure 5.27: Variation of angle of attack for different number of blades.

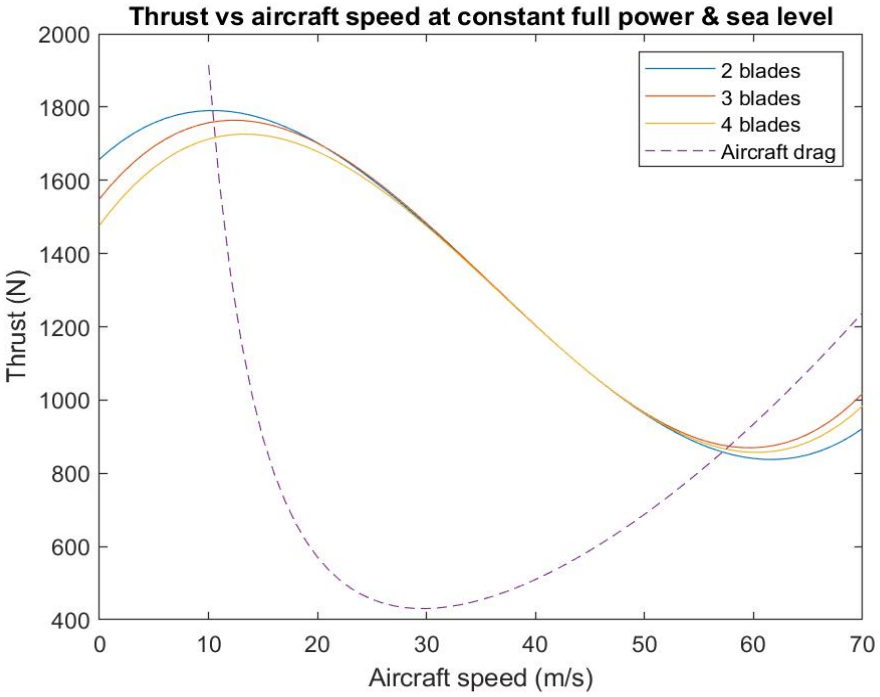

Figure 5.28: Thrust at full power versus aircraft speed for different number of blades.

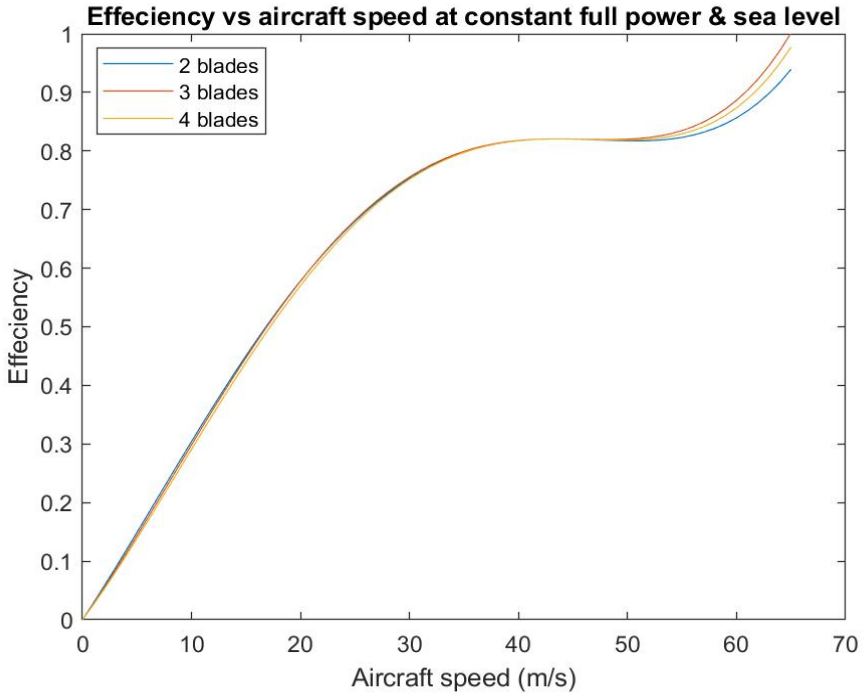

Figure 5.29: Propeller efficiency at constant full power for different number of blades.

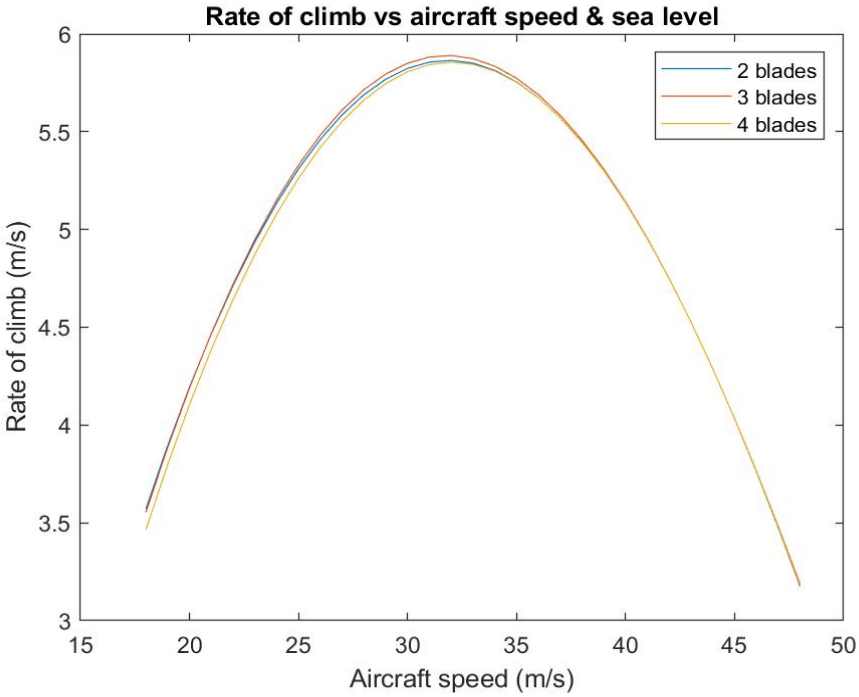

Figure 5.30: Rate of Climb of the aircraft at for different number of blades at sea level.

Chapter 6

Conclusions and future work

6.1 Conclusions

The present design method investigation reached the following conclusion:

1- The new propeller design has a higher max speed than Pipistrel Alpha Electro at design point with speed 4.2 km/h, 6.7 km/h, and 5.3 km/h for 2, 3, and 4 blades, respectively. It is a valuable initial improvement for the current propeller.

2- Clark Y propeller thrust is higher than RAF 6 propeller thrust by 3.1 N at the design point.

3- RAF 6 airfoil consumed 28.85 kWh in cruise-phase at sea level while Clark Y airfoil consumed 29.05 kWh, which in terms of range equals 0.67 Km/h. This result is considered as a small increase.

4- The variable pitch propeller consumed less power by 0.14 kWh compare to the fixed pitch propellers at cruise speed and altitude 3000 m, and the propeller efficiency increased by 0.4%. This improvement is limited in comparison with the change from fixed pitch to variable pitch propeller.

5- Increasing the number of blades does not signify a reduction in the propeller efficiency where the optimum blade number for the design specifications is 3 blades.

6- The highest thrust obtained by utilizing 3 blades.

6.2 Future work

Based on the current conclusions, it is suggested that the next step in this research focuses on investigating the variable pitch propeller more in detail by studying the performance improvement in the climb phase, the influence of different airfoils, and the effects of various flight speeds. Also, investigate in a wide range the effect of engine power, RPM, and propeller diameter on the optimum number of blades.

Bibliography

[1] EASA. “European Aviation Environmental Report”. In: *European Union Aviation Safety Agency* (2019). URL: https://www.easa.europa.eu/eaer/.

[2] Airbus. “Thermal Engines vs. Electric Motors”. In: *Airbus Website* (2019). URL: https://www.airbus.com/newsroom/stories/airbus-pursues-hybrid-propulsion-solutions-for-future-air-vehicles.html.

[3] L. Kumar and Sh. Jain. “Electric Propulsion System for Electric Vehicular Technology: a Review”. In: *Renewable and Sustainable Energy Reviews* (2014), pp. 924–940.

[4] J. Fehrenbacher, D. Stanley, M. Johnson, and J. Honchell. “Electric Motor & Power Source Selection for Small Aircraft Propulsion”. In: *College of Technology Directed Projects,* 33 (2011).

[5] M. Hepperle. “Electric Flight – Potential and Limitations”. In: *AVT-209 Workshop on Energy Efficient Technologies and Concepts Operation* (2012).

[6] S. Ma, S. Wang, C. Zhang, and S. Zhang. “A method to improve the efficiency of an electric aircraft propulsion system”. In: *Energy,* 140 (2017), pp. 436–443.

[7] S. Wang, S. Zhang, and S. Ma. “An Energy Efficiency Optimization Method for Fixed Pitch Propeller Electric Aircraft Propulsion Systems”. In: *IEEE Access,* 7 (2019), pp. 159986–159993.

[8] G. Romeo, E. Cestino, M. Pacino, F. Borello, and G. Correa. “Design and testing of a propeller for a two-seater aircraft powered by fuel cells”. In: *J. Aerospace Engineering,* 226,7 (2011), pp. 804–816.

[9] S. Xiang, Y. Liuand G. Tong, W. Zhao, S. Tong, and Y. Li. “An improved propeller design method for the electric aircraft”. In: *Aerospace Science and Technology,* 78 (2018), pp. 488–493.

[10] H. Glauert. “Airplane Propellers”. In: *Aerodynamic Theory. Springer, Berlin, Heidelberg* (2019), pp. 169–360.

[11] *Solar Impulse Foundation*. 2016. URL: https://www.easa.europa.eu/eaer/.

[12] R. Glassock, M. Galea, W. Williams, and T. Glesk. “Hybrid Electric Aircraft Propulsion Case Study for Skydiving Mission”. In: *MDPI Aerospace* (2017).

[13] K. Takahashi, H. Fujimoto, Y. Hori, H. Kobayashi, and A. Nishizawa. “Modeling of Propeller Electric Airplane and Thrust Control Using Advantage of Electric Motor”. In: *2014 IEEE 13th International Workshop on Advanced Motion Control (AMC), Yokohama* (2014), pp. 482–487.

[14] O. Yetik and T. H. Karakoc. “A Numerical Study on the Thermal Performance of Prismatic Li-Ion Batteries for Hybrid Electric Aircraft”. In: *Energy,* 195 (2020).

[15] J. G. Kim, B. Sonand S. Mukherjee, N. Schuppert, A. Bates, O. Kwon, M. J. Choi, H. Y. Chung, and S. Park. “A Review of Lithium and Non-Lithium Based Solid State Batteries”. In: *J. Power Sources,* 282 (2015), pp. 299–322.

[16] A. Betz. “Schraubenpropeller mit Geringstem Energieverlust”. In: *Königliche Gesellschaft der Wissenschaften, Göttingen Mathematisch-Physikalische Klasse* (1919), pp. 193–217.

[17] E.E. Larrabee. “Practical design of minimum Induced Loss Propellers”. In: *Business Aircraft Meeting and Exposition Wichita, SAE Preprint 790585* (1979).

[18] S. Goldstein. “On The Vortex Theory of Screw Propellers”. In: *Proc. of the Royal Society A 123* (1929), pp. 440–465.

[19] R. Eppler and M. Hepperle. “A Procedure For Propeller Design by Inverse Methods”. In: *Proceedings of the International Conference on Inverse Design Concepts in Engineering Sciences (ICIDES), Austin TX,October 17-18* (1984).

[20] T. Theodorsen. “Theory of Propellers”. In: *New York: McGraw-Hill Book Company* (1984), p. 164.

[21] Q. R. Wald. “The Aerodynamics of Propellers”. In: *Progress in Aerospace Sciences,* 42,2 (2006), pp. 85–128.

[22] S. D’Angelo, F. Berardi, and E. Minisci. “Aerodynamic Performances of Propellers with Parametric Considerations on the Optimal Design”. In: *The Aeronautical Journal,* 106,1060 (2002), pp. 313–320.

[23] X. Zheng, X. Wang, Z. Cheng, and D. Han. “The Efficiency Analysis of High-Altitude Propeller Based on Vortex Lattice Lifting Line Theory”. In: *The Aeronautical Journal,* 121,1236 (2017), pp. 141–162.

[24] J. Cho and S. Lee. “Propeller Blade Shape Optimization for Efficiency Improvement”. In: *Computers & Fluids,* 27,3 (1998), pp. 407–419.

[25] J. A. Lieser, D. Lohmann, and C. H. Rohardt. “Aeroacoustic Design of A 6-Bladed Propeller”. In: *Aerospace Science and Technology,* 1,6 (1997), pp. 381–389.

[26] O. Gur and A. Rosen. “Optimization of Propeller Based Propulsion System”. In: *Journal of Aircraft,* 46,1 (2009).

[27] S. Xiang, WP. Zhao, LG. Zhang, and G. Tong. “A Method Combined with the Genetic Algorithm for Design of High Efficiency Propeller”. In: *Applied Mechanics and Materials,* 709 (2014), pp. 172–175.

[28] M. Stuhlpfarrer, A. Valero-Andreu, and C. Breitsamter. “Numerical and Experimental Investigations of the Propeller Characteristics of An Electrically Powered Ultralight Aircraft”. In: *CEAS Aeronautical Journal,* 8 (2017), pp. 441–460.

[29] Y. Wu, YT. Ai, W. Ze, T. Jing, X. Song, and Y. Chen. “A Novel Aerodynamic Noise Reduction Method Based on Improving Spanwise Blade Shape for Electric Propeller Aircraft”. In: *International Journal of Aerospace Engineering,* 2019, Article ID 3750451 (2017).

[30] W. Rankine. “On the Mechanical Principles of the Action of Propellers”. In: *Transactions of the Institute of Naval Architects 6,* (1865), pp. 13–39.

[31] R. Froude. “On the Part Played in Propulsion by Difference in Fluid Pressure”. In: *Transactions of the Institute of Naval Architects 30* (1889), pp. 390–405.

[32] E. Bratt. *Aircraft Propellers Design and Analysis,* 2nd ed. Flygföretag HB, 1991.

[33] E. P. Hartman and D. Biermann. “The Aerodynamic Characteristics of Full-Scale Propellers Having 2, 3, And 4 Blades of Clark Y and R. A. F. 6 Airfoil Sections”. In: *National Advisory Committee for Aeronautics,* Report No. 640 (1938).

[34] D. Biermann and E. P. Hartman. “The Aerodynamic Characteristics of Six Full-Scale Propellers Having Different Airfoil Sections”. In: *National Advisory Committee for Aeronautics,* Report No. 650 (1939), pp. 145–178.

[35] A. M. P. Gordillo. “Comparison between Semiempirical and Computational Techniques in the Prediction of Aerodynamic Performance of the Rotor of a Quadcopter”. In: *National Advisory Committee for Aeronautics,* (2017).

[36] W. A. Welch. *Lightplane Propeller Design, Selection, Maintenance & Repair*. 1st ed. Tab Books, 1979.

[37] S. Gudmundsson. *General Aviation Aircraft Design: Applied Methods and Procedures*. 1st ed. Butterworth-Heinemann, 2014.

[38] E. Torenbeek. *Synthesis of subsonic airplane design*. 1st ed. Delft University Press, 1982.

[39] B. H. Carson. “Fuel Efficiency of Small Aircraft”. In: *J. Aircraft,* 19,6 (1982).

[40] S. Slavik, J. Klesa, and J. Brabec. “Propeller Selection by Means of Pareto-Optimal Sets Applied to Flight Performance”. In: *Aerospace,* 7,21 (2020).

[41] Pipistrel. “Aircaft Information Pipistrel Alpha Electro”. In: *Pipistrel-USA* (2017).

[42] Pipistrel. “Pilot’s Operating Handbook, Applies to all Alpha Electro Aircraft Equipped with 60 kW Electric Motor”. In: *Pipistrel-EU, Slovenia* (2017).

[43] P.B. MacCready, P.B.S. Lissaman, W.R. Morgan, and J.D. Burke. “Sun-powered aircraft design”. In: *J. Aircraft 6,* 20 (1983), pp. 487–493.

[44] Hartzell Propeller. “What’s the difference between a fixed pitch and variable pitch propeller?” In: *Hartzell Propeller Website,* (2016). URL: https://hartzellprop.com/whats-the-difference-between-a-fixed-pitch-and-variable-pitch-propeller/.

[45] “Private conservation with the Aerodynamics Engineer”. In: *Pipistrel aircraft manufacturer* (2020).

[46] M. Hepperle. “Selecting an Equivalent Multi-Blade Propeller”. In: *Martin Hepperle Website,* (1996). URL: https://www.mh-aerotools.de/airfoils/propuls2.htm.

Appendix A

Appendix

A.1 RAF 6 airfoil Propeller performance at various altitudes

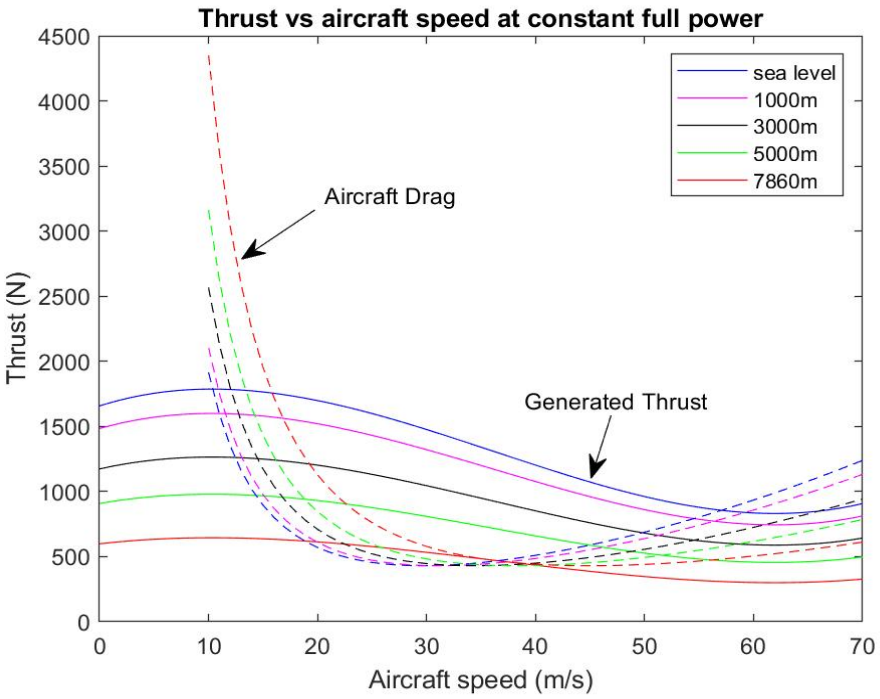

Figure A.1: Thrust at constant full power versus aircraft speed for various altitudes.

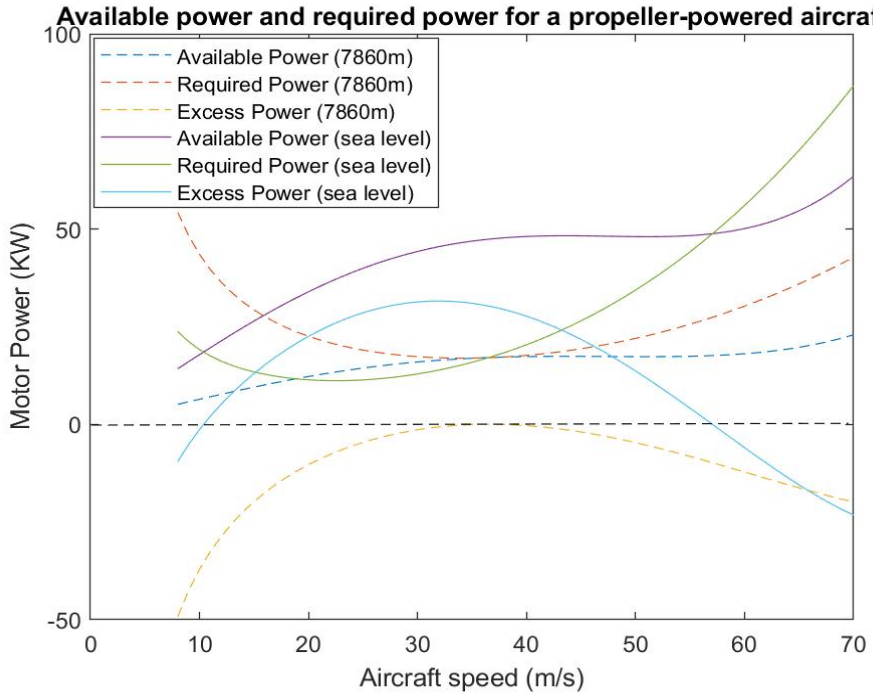

Figure A.2: Engine power versus aircraft speed at max and min altitudes.

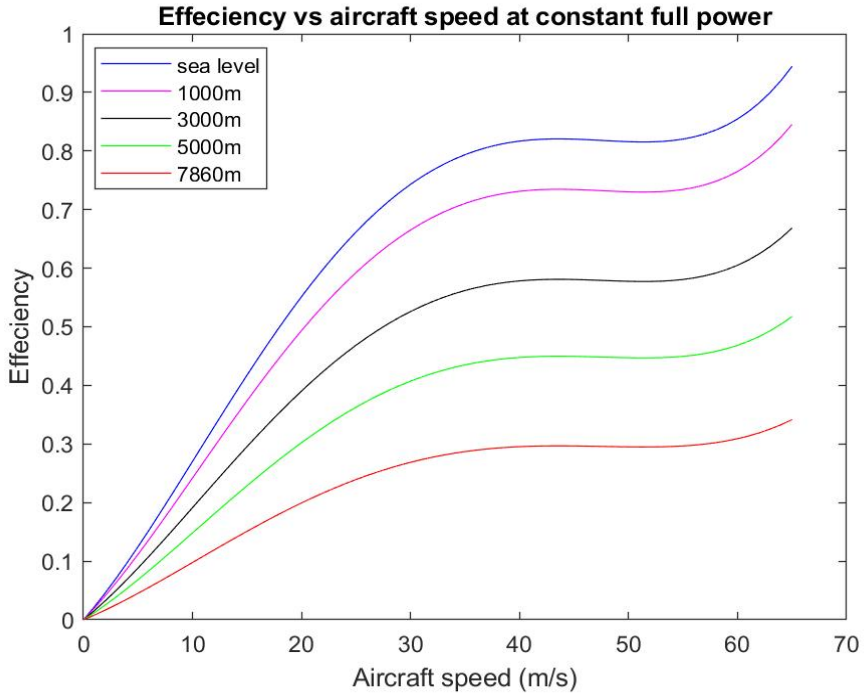

Figure A.3: Propeller efficiency versus aircraft speed for various altitudes.

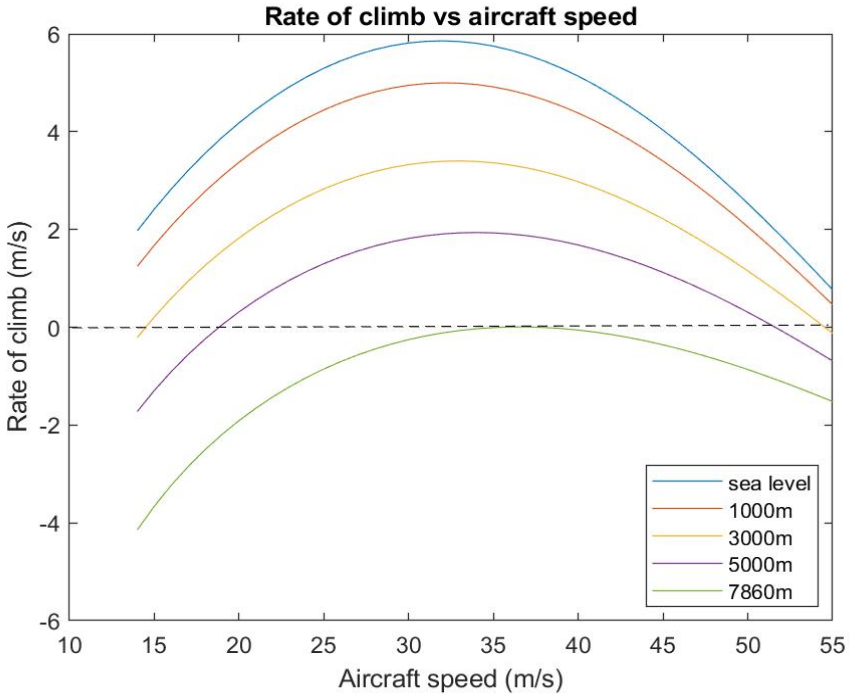

Figure A.4: Rate of Climb of the aircraft at various altitudes.